

Using field data to constrain a numerical kinematic model for ridge-transform deformation in the Troodos ophiolite, Cyprus

Chelsea P. Scott¹, Sarah J. Titus^{1*}, and Joshua R. Davis²

¹DEPARTMENT OF GEOLOGY, CARLETON COLLEGE, ONE NORTH COLLEGE STREET, NORTHFIELD, MINNESOTA 55057, USA

²DEPARTMENT OF MATHEMATICS, CARLETON COLLEGE, ONE NORTH COLLEGE STREET, NORTHFIELD, MINNESOTA 55057, USA

ABSTRACT

The Troodos ophiolite in Cyprus provides a unique opportunity to examine spatially varying patterns of deformation near a ridge-transform intersection. We focus on the paleo-inside corner defined by the E-W-striking, dextral Arakapas transform fault and the N-S-striking Solea graben. Rocks within the inside corner are primarily sheeted dikes and gabbros. The strikes of dikes vary with proximity to the Arakapas fault, changing from NW- to N- to E-striking with increasing proximity to the fault. We report new paleomagnetic results from 24 stations in the gabbroic rocks. When augmented with data from several previous studies, the combined paleomagnetic data set indicates that vertical-axis rotations increase from 5° to 90° with distance from the Solea graben. Rotations are also largest near the transform fault.

We develop numerical kinematic models for deformation within the inside corner based on these field data. First, we fit an interpolation function to the two-dimensional field of vertical-axis rotations. This field is then used to undeform dikes, assuming that dikes were either part of rigid blocks or passive markers within a continuum. We find that dikes return to a consistent NW to NNW strike throughout much of the inside corner. This initial orientation is not ridge-parallel and therefore different from most common assumptions of dike behavior in Cyprus. However, the orientation is consistent with predictions from dynamic models of heterogeneous stress directions that develop near ridge-transform intersections.

LITHOSPHERE, v. 5, no. 1; p. 109–127 | Published online 14 November 2012

doi: 10.1130/L237.1

INTRODUCTION

Ridge-transform intersections in mid-ocean spreading centers are complex regions of deformation: Rocks are affected by spreading at the ridge as well as shearing along the transform fault. In modern ridge-transform intersections, where the shallowest crustal depths can be observed directly on the seafloor, the curvature of structures such as abyssal hills, ridge segments, and fault scarps within the inside corner (e.g., Crane, 1976; Schouten et al., 1980; Searle, 1983; Fox and Gallo, 1984; MacDonald et al., 1986; Fornari et al., 1989; Livermore et al., 1991; Sonder and Pockalny, 1999; Croon et al., 2010) is often taken as evidence for these overlapping styles of deformation. To understand how ridge-transform deformation is accommodated at deeper lithospheric levels, other approaches must be employed because direct observation is impossible.

One common approach is to build dynamic models exploring the effects of various mechanical and thermodynamic parameters within ridge-transform intersections (e.g., Fujita and Sleep, 1978; Furlong et al., 2001;

Behn et al., 2002; Ligi et al., 2002; van Wijk and Blackman, 2005; Behn et al., 2007). This approach often focuses on the instantaneous view of deformation, presenting a snapshot of the stress and/or velocity field as a way to illustrate the model results. In a dextral transform, for example, most models predict left-leaning, maximum horizontal stress directions in the inside corner (Figs. 1A and 1B; e.g., Phipps Morgan and Parmentier, 1984; Grindlay and Fox, 1993; Långbacka and Gudmundsson, 1995; Neves et al., 2004). These stress directions often compare favorably with the deflection of lineaments in modern oceanic systems (Fig. 1C; e.g., Fox and Gallo, 1984).

Ridge-transform systems have also been studied directly using exceptional exposures within ophiolites (Simonian and Gass, 1978; Prinzhofer and Nicolas, 1980; Smewing, 1980; Suhr and Cawood, 2001; Abelson et al., 2002; Granot et al., 2006; Titus et al., 2011) and in rare on-land exposures in Iceland (Young et al., 1985; Jancin et al., 1995). This field-based approach often examines how fabrics, microstructures, paleomagnetic data, etc., vary through the inside corner (Figs. 1D and 1E). These types of field observations reflect the final state of a protracted history of deforma-

tion, as opposed to the instantaneous view. In a dextral system, field studies reveal right-leaning fabrics, often delineated by changing dike strikes, within the inside corner. The sense of deflection matches observations from shear zones at all scales of observations (Fig. 1F).

Despite matching reasonable natural analogues, these two approaches produce opposite senses of curvature for the same sense of fault motion, even when using the same kind of marker, such as dike orientations. In large part, the disagreement is due to the disparate time scales observed in the two approaches. In this study, we attempt to bridge the gap between these two approaches by working backward from field data (i.e., the finite view) to predict the possible initial state (i.e., the instantaneous view). Our analysis is based on data from a ridge-transform intersection preserved in the Troodos ophiolite in Cyprus, and relies on a numerical kinematic model to move between the finite and instantaneous views of deformation. Our results have implications for the interpretation of the ridge-transform system in Cyprus, in particular, as well as serving as a model for how to more quantitatively link field data to model predictions in a complexly deforming region.

*E-mail: stitus@carleton.edu.

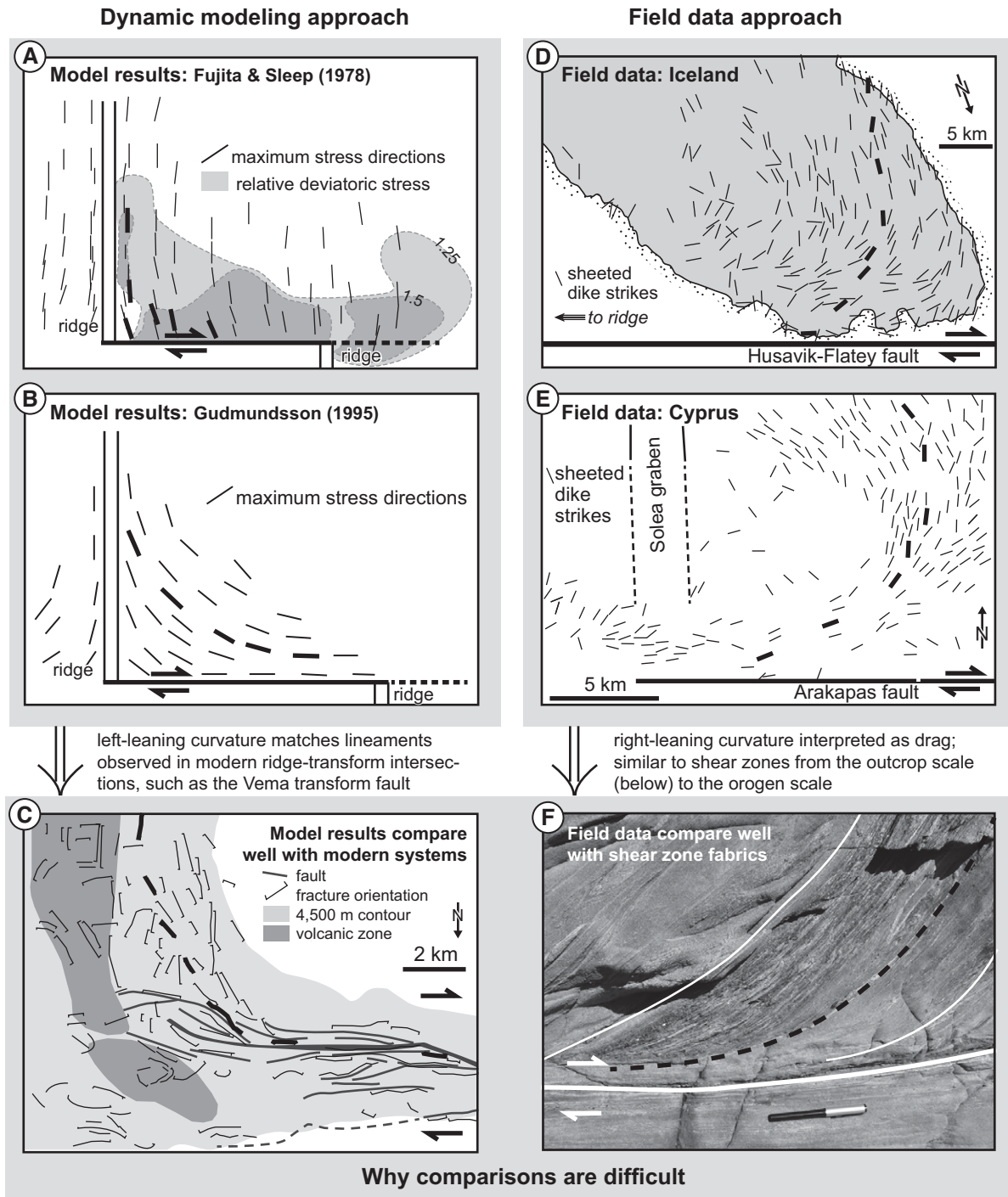


Figure 1. Diagrams designed to illustrate two common approaches to studying ridge-transform intersections. The left column represents the instantaneous view of deformation, showing the maximum stress directions from the dynamic models of (A) Fujita and Sleep (1978) and (B) Gudmundsson (1995). Left-leaning features within the inside corner of these models match left-leaning lineaments in a modern ridge-transform intersection shown in (C), modified from MacDonald et al. (1986). The right column represents the finite view of deformation, showing sheeted dike strikes from field examples in (D) Iceland from Young et al. (1985) and (E) in Cyprus from our Figure 2 (and citations therein). Right-leaning features for these inside corners match patterns expected in shear zones, such as the photograph in (F). Photo credit belongs to Manish Mamtani. In all panels, the bold black lines highlight the sense of curvature. The two common approaches produce the exact opposite sense of curvature in dextral systems, making comparisons between them difficult.

GEOLOGIC SETTING

The Troodos ophiolite formed in a supra-subduction-zone environment (Miyashiro, 1973; Pearce et al., 1984) during the Late Cretaceous (Blome and Irwin, 1985; Mukasa and Ludden, 1987). While there are different tectonic models for the collision that led to ophiolite emplacement (Moores et al., 1984; Clube et al., 1985; Clube and Robertson, 1986; MacLeod, 1990; Murton, 1990; Malpas et al., 1993), all models include an $\sim 90^\circ$ counterclockwise rotation by the early Eocene. This rotation resulted in a well-defined mean Troodos paleomagnetic direction that is nearly due west in present-day coordinates (Clube et al., 1985). Unlike other Tethyan ophiolites (Robertson, 2002), the Troodos ophiolite shows no major deformation related to emplacement (Moores and Vine, 1971; Gass, 1990; Robinson and Malpas, 1990). Mild doming and postemplacement erosion expose the complete ophiolite stratigraphy (Moores and Vine, 1971), including large expanses through the sheeted dike complex that were critical to the development of early ideas in plate tectonics (Gass, 1968; Anonymous, 1972; Kidd and Cann, 1974; Robinson et al., 2008).

Three parallel, N-S-striking ridge segments are exposed in the crustal section of the ophiolite, known as the Solea, Mitsero, and Larnaca grabens (see inset in Fig. 2; Varga and Moores, 1985). Of the three, the Solea graben seems to be the most prominent ridge, where spreading was accommodated by a combination of magmatic accretion and minor normal faulting and tilting (Varga and Moores, 1985; Allerton and Vine, 1991; Hurst et al., 1994). The Mitsero graben is interpreted as reflecting off-axis magmatism (e.g., van Everdingen and Cawood, 1995), while the Larnaca graben is considered to reflect late-stage spreading after a ridge jump to the east (Allerton and Vine, 1991).

The ophiolite also has a major E-W-striking valley, interpreted as a paleotransform fault (Simonian and Gass, 1978; Murton and Gass, 1986; Allerton and Vine, 1992; MacLeod and Murton, 1993; Gass et al., 1994). This 35-km-long feature, known as the Arakapas fault or Southern Troodos transform fault, ranges in width from 0.5 to 1.5 km, and is characterized by a significant topographic low and highly deformed rocks (Simonian and Gass, 1978). Because the ophiolite was not subaerially exposed and eroded until Pliocene–Quaternary time (Robertson and Xenophonotos, 1993), the topography in the transform belt is interpreted to reflect original seafloor topography.

ARAKAPAS FAULT MOTION

One of the most striking features related to the Arakapas transform system is the curvature

of sheeted dikes north of the fault and east of the ultramafic exposures (Fig. 2). The classic description for these dike orientations (Simonian and Gass, 1978), reiterated in numerous other publications, is that their strikes rotate in a clockwise sense from N- to NE- to E-striking with increasing proximity to the fault. However, we note that in the slightly expanded view of the region in Figure 2, many of the dikes farthest from the fault are actually NW-striking (not N-S-striking), for example, near the town of Kakopetria.

The dike curvature is one of the best available data sets for determining motion along the Arakapas fault, since conflicting shear sense indicators are observed within the fault zone (Gass et al., 1994; MacLeod and Murton, 1995). However, there are two possible interpretations for the dike curvature, which resulted in debate on the sense of fault motion during the 1980s and 1990s. Some workers suggested that dikes recorded the heterogeneous stress field at the time of emplacement and experienced no deformation following intrusion (Varga and Moores, 1985; Murton, 1986; Dilek et al., 1990). This is essentially the dynamic modeling viewpoint mentioned in the Introduction. Interpreted in this light, the curvature matches the mirror image of the modeling results in Figure 1, suggesting sinistral motion along the fault. Other workers suggested a classic kinematic interpretation, where the curvature developed over time due to drag along the transform fault (Simonian and Gass, 1978). For this alternative interpretation, workers assumed that sheeted dikes initially intruded N-S, parallel to the ridge, and then rotated clockwise as they moved away from the ridge due to distributed dextral deformation adjacent to the Arakapas fault. The sense-of-motion debate was eventually settled (MacLeod and Murton, 1995) when independent paleomagnetic data demonstrated clockwise rotations consistent with dextral motion (Bonhommet et al., 1988; Allerton and Vine, 1990; MacLeod et al., 1990; Morris et al., 1990).

This dextral interpretation implies that the region between the Arakapas fault and the Solea graben preserves a paleo-inside corner. The rocks in this region are primarily sheeted dikes and gabbros, allowing us to investigate deeper lithospheric patterns of deformation than those from exposures of ridge-transform systems in Iceland or on the seafloor. A rich geologic data set already exists for this region (summarized in Fig. 2), including hundreds of sheeted dike orientations and tens of paleomagnetic measurements. In the following two sections, we discuss our additions to both dike and paleomagnetic data sets along with spatial patterns observed within those data sets.

DIKE ORIENTATIONS

Data Compilation

We compiled dike orientations from several published maps. Those from the Cyprus Geological Survey at the 1:31,680 scale (Bishopp et al., 1959; Bear, 1960; Bear and Carr, 1960; Bear and Morel, 1960; Pantazis, 1967) provided coverage over most of the region shown in Figure 2. Four of the five relevant maps included the strike and dip of sheeted dikes. However, the Peristrona sheet, covering much of the NE portion of Figure 2, only contained strike information, except where vertical dikes were denoted by a separate symbol. Data from the 1:25,000 scale map from Gass et al. (1994) were also included, since this more detailed mapping provides critical information near the transform fault.

All of these published maps included the strikes of a variety of other features such as dikes within the upper-crustal units, quartz porphyry and granophyric sheets within the sheeted dike complex, picrite dikes, and microgabbroic sheets in the gabbros. We included these additional features in our overall dike data set because they are often available where sparse sheeted dike orientations are found.

We augmented this large data set with our own measurements of ~ 500 dike orientations collected from 64 stations. The station locations are indicated in Figure 2, and are concentrated near the likely positions of the ridge-transform intersection and within the inside corner. At each of our sites, there may be as few as one dike orientation or as many as 20.

In total, our data set includes the orientation of ~ 3600 features with strike values providing a detailed, two-dimensional data set. Of these, ~ 1900 also had associated dip values, resulting in a smaller, three-dimensional data set.

Dike Orientation Analysis

To examine and quantify spatial variability in dike orientations, we divided the map region from Figure 2 into 160 blocks (Fig. 3A). Block boundaries are based on mapped faults and/or lithological contacts. Block sizes were chosen to ensure that there were at least four dikes per block. Two-dimensional dike orientations were averaged for each block (Fig. 3A), and three-dimensional orientations were grouped for multiple adjacent blocks and plotted on stereographic projections (Fig. 3B).

Both panels in Figure 3 highlight the variability of dike orientations on either side of the ultramafic rocks. On the west side, dikes tend to strike N-S, with moderate dips to the E. This pattern is altered somewhat near the transform

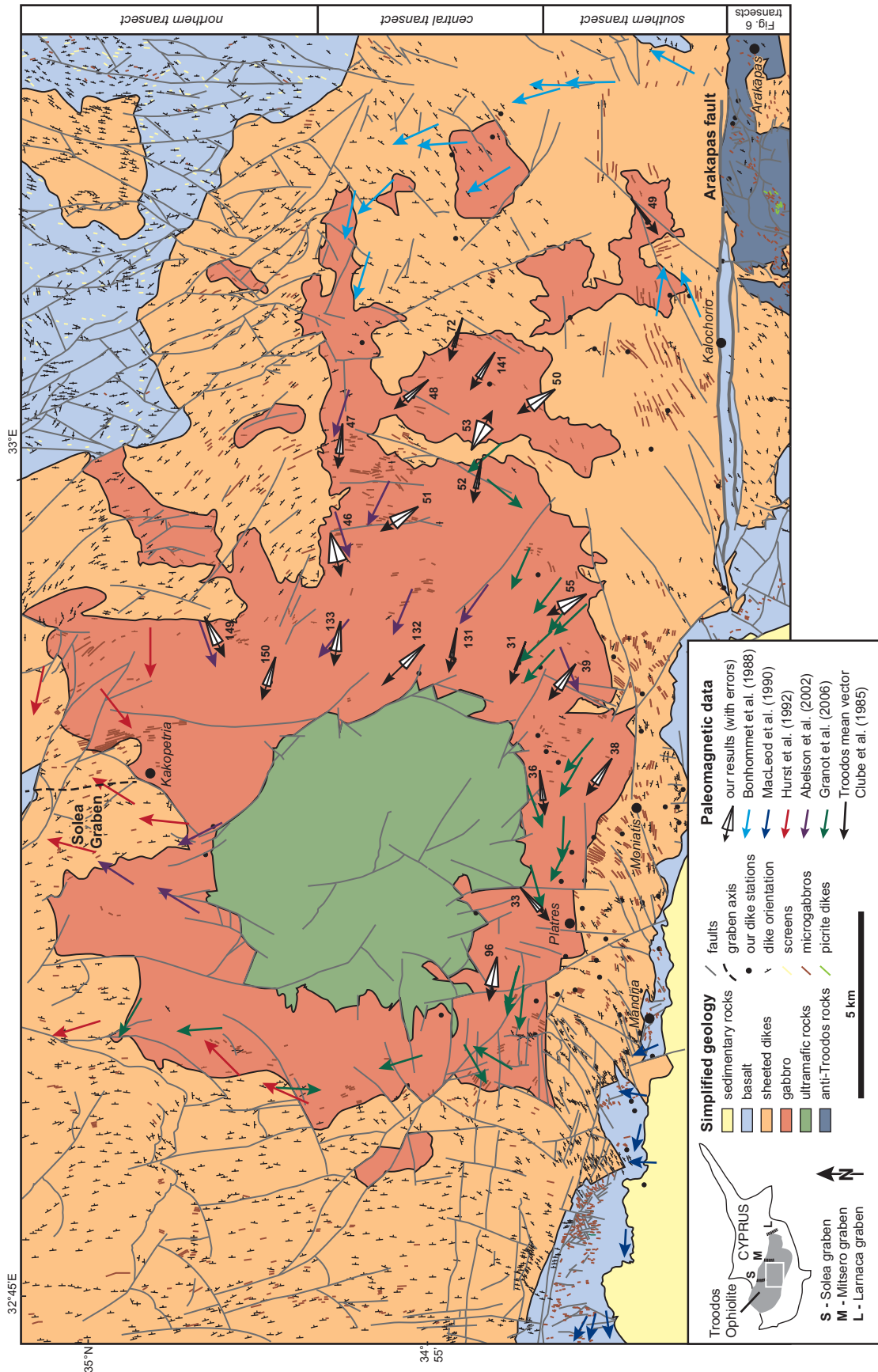


Figure 2. Simplified geologic map for the ridge-transform intersection in the Troodos ophiolite. Map details are modified from Bishopp et al. (1959), Bear and Morel (1960), Bear and Carr (1960), Bear (1960), Pantazis (1967), and Gass et al. (1994). Axis of the Solea Graben axis is from Hurst et al. (1992). Inset shows the position of this map box within the country of Cyprus and the locations of the Solea, Mitsero, and Lamaca grabens. Paleomagnetic results from several studies have been compiled on this map. The divisions used for paleomagnetic transects in Figure 6 are indicated on the right side of the map.

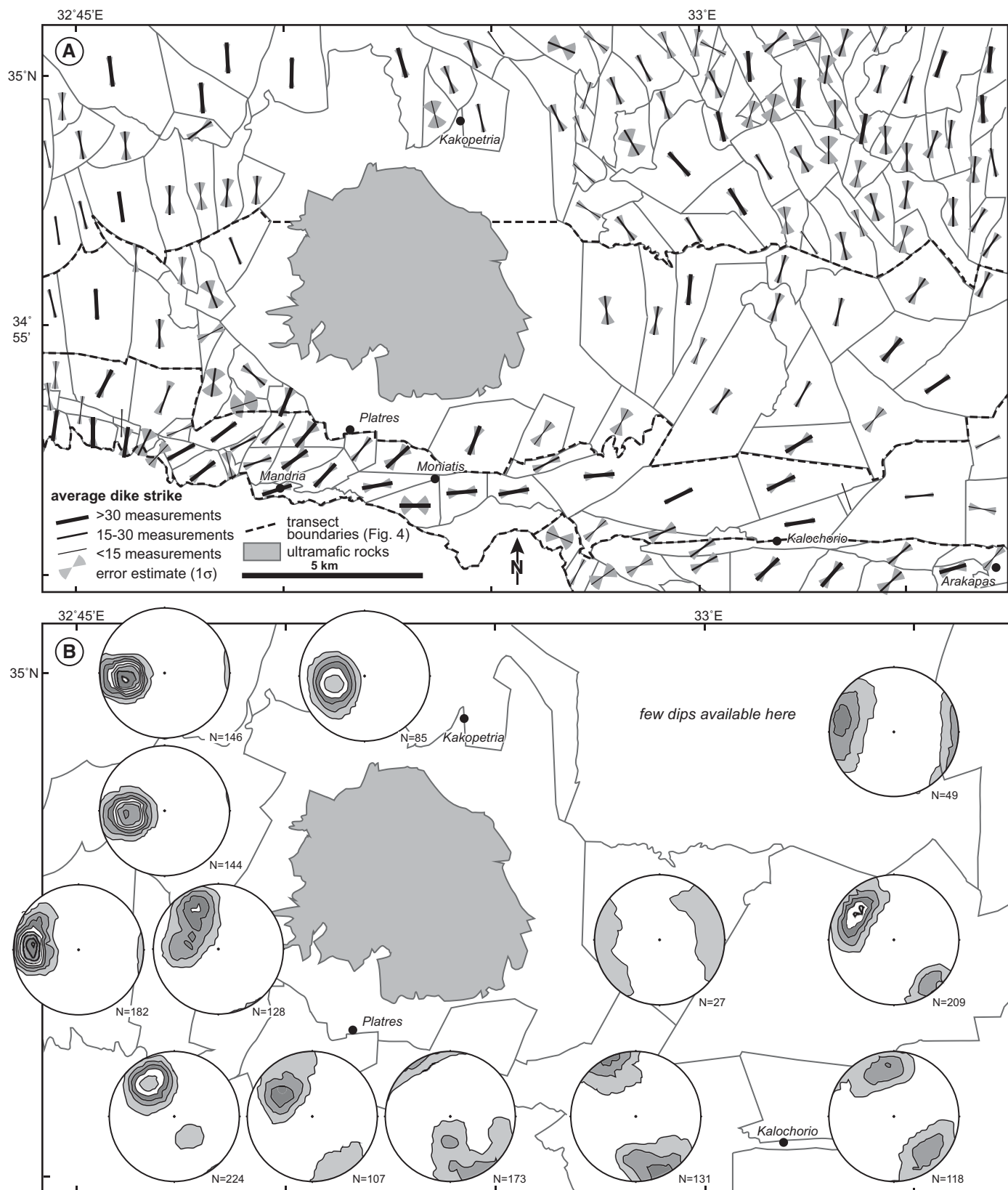


Figure 3. (A) Two-dimensional dike orientations for 160 blocks making up the same region shown in Figure 2. The line in the center of each block shows the average strike of dikes in that block; the line thickness corresponds to the number of data used to compute the average. The wedges illustrate the 1σ variability around the mean orientation. No dip information was used in this calculation. **(B)** Three-dimensional dike orientations for groups of adjacent blocks. All stereographic projections illustrate poles to dikes on lower-hemisphere, equal-area projections with 4σ Kamb contours.

fault, where dike strikes change to a NNE direction. South of the ultramafic exposures and along the Arakapas fault, dikes are steeply dipping in both directions and generally NE-striking or E-striking. On the east side, dikes are steeply dipping in both directions with NW strikes close to the ultramafic rocks to NE strikes farther east.

Figure 4 also highlights the differences in dike populations between the west and east sides of the map while providing a more quantitative view of orientation changes along several E-W transects. The arrows in this diagram are meant to highlight broad trends away from inflection points in dike behavior, which presumably mark the position of the paleoridge. Our descriptions of the transect patterns in the following discussion mimic these arrows.

On the west side of each transect, the strikes and dips of dikes change with position, generally rotating counterclockwise toward the west and steepening. The change in strike direction is smallest along the northern profile ($\sim 10^\circ$), where most dikes' strikes are subparallel to the inferred ridge strike (Fig. 4A), and largest along the southern profile ($\sim 60^\circ$), where only dikes farthest west parallel the inferred ridge strike (Fig. 4C). The patterns for the east side of the profiles are more variable. For the northern and central profiles, dike strikes rotate clockwise by up to 90° toward the east, but their actual azimuthal values are different. In the north, the easternmost dikes have strikes of 030° (Fig. 4A) compared to 060° in the central profile (Fig. 4B). For the southern and transform profiles (Fig. 4C and 4D), dikes have more consistent orientations with steep ENE strikes, especially between the 20 and 35 km marks on the graph.

PALEOMAGNETIC DATA

Data Compilation

We compiled results from five previous regional paleomagnetic studies on Figure 2. These values reflect the studies' in situ results prior to any corrections made by the original authors for tilting and/or rotation. Paleomagnetic data from each site can be compared to the well-defined Troodos mean vector, which has a declination of 274° and an inclination of 36° (Clube et al., 1985). This mean vector serves as a reference for the undeformed state; deviations in declination and inclination are assumed to reflect deformation of the rocks in question.

Three prior studies sampled rocks from the sheeted dike complex. MacLeod et al. (1990) reported results for 11 stations in the far southwest of Figure 2. Hurst et al. (1992) reported data from 22 stations in the Solea graben (many sites are outside of the map region in Fig. 2).

Bonhommet et al. (1988) collected data from 13 sites in the southeast portion of the map, along a transect perpendicular to the Arakapas fault.

Two more recent studies reported paleomagnetic results within the gabbros. Abelson et al. (2002) collected data from 11 sites east of the ultramafic rocks. Granot et al. (2006) reported results from 23 sites located on the western, southern, and eastern margins of the ultramafic rocks.

The two studies of gabbroic rocks both demonstrate that AF (alternating field)-demagnetization is suitable for paleomagnetic analysis and that magnetite is the carrier of the magnetic signal. We follow their methods, augmenting the gabbroic data set with samples from 32 additional sites collected east of the ultramafic rocks (Fig. 2). Two hand samples were collected from outcrops with no significant secondary or hydrothermal alteration. These rocks were cored and oriented in the laboratory. Their remanent magnetization was measured using AF-demagnetization at the University of Minnesota's Institute for Rock Magnetism. For each station, five to seven specimens were step-wise demagnetized from 5 mT to 200 mT in steps of 5 mT at low fields and steps of 30–50 mT at high fields.

Most samples contained a stable primary and often a secondary magnetic component. Best-fit lines to the primary demagnetization steps were calculated using principal component analysis (Kirschvink, 1980; Jones, 2002). Two representative demagnetization paths are shown in Figure 5. Only specimens with a maximum angle of deviation about the principal component direction of $<5^\circ$ were included in our final analysis, yielding data from 24 sites of the original 32 sites. The mean characteristic remanent magnetization (ChRM) direction for each specimen and the station mean magnetization vector were computed using Fisher statistics. The results from each site are plotted on Figure 2 and summarized in Table 1.

Paleomagnetic Data Analysis

Similar to our analysis of dike orientations, we examine patterns of the paleomagnetic data in map view (Fig. 2) as well as along three E-W-striking transects (Fig. 6). These two different views provide complementary information about spatial gradients in the ChRMs.

In map view, there are clear differences in declination directions for regions north, west, south, and east of the ultramafic exposures. Sites to the north and west tend to show either N- or S-trending declinations. Most sites south of the ultramafic rocks are W-directed, subparallel to the Troodos mean vector. Those east of the

ultramafic rocks are typically NW-directed, suggesting varying degrees of clockwise rotations.

In profile view, we examine changes in declination and inclination along a northern, central, and southern transect (see Fig. 2 for transect locations). These transects are close to, but do not perfectly match, the divisions used for the dike profiles (Fig. 4) due to differences in data spacing and availability. On this plot, we show the in situ results of paleomagnetic studies, which have not been corrected for tilting or rotation.

Most of the data along the northern profile are from Hurst et al. (1992), whose study was designed to examine differences on either side of the Solea graben. The westernmost sites have large declination and inclination variations, whereas the easternmost sites are generally parallel to the Troodos mean vector. Hurst et al. (1992) primarily sampled from the sheeted dike complex, but the few stations from gabbros match the overall pattern along this transect.

Data from the central profile are predominantly from gabbros. The western sites have declinations near the Troodos mean vector direction with variable inclinations. These results suggest rotations about subhorizontal axes parallel to the paleoridge. From the 17 km mark, the magnitude of clockwise declination deflection increases by 60° toward the east. Although the associated inclinations show scatter, there seems to be no consistent pattern in their deflection.

Along the southern profile, the western sites are mostly from the sheeted dike complex. Those sites farthest west parallel the Troodos mean vector (0–1 km), while their nearest neighbors (5–8 km) show large clockwise rotations in declination. Clockwise rotation is also observed in sites from the gabbroic rocks, although this occurs farther east (13–21 km) and is associated with consistent inclination shallowing. The easternmost sites show large clockwise rotation of up to 90° accompanied by significant steepening of the ChRMs. In order to achieve these patterns along the east side of transect, rocks either underwent multistep deformation involving tilting and vertical-axis rotation or they were rotated about plunging axes.

Three important conclusions can be drawn from our compilation of paleomagnetic data. First, the data from our 24 sites match those of other regional studies, suggesting that our paleomagnetic results are robust. Second, data from the sheeted dikes often match the patterns in the gabbros, except possibly along the southern transect nearest the Arakapas fault, suggesting that both rock types generally experienced the same kind of deformation patterns. Third, for sites along the central profile where the most complete paleomagnetic data set exists, the inclination values cluster near the Troodos mean vector

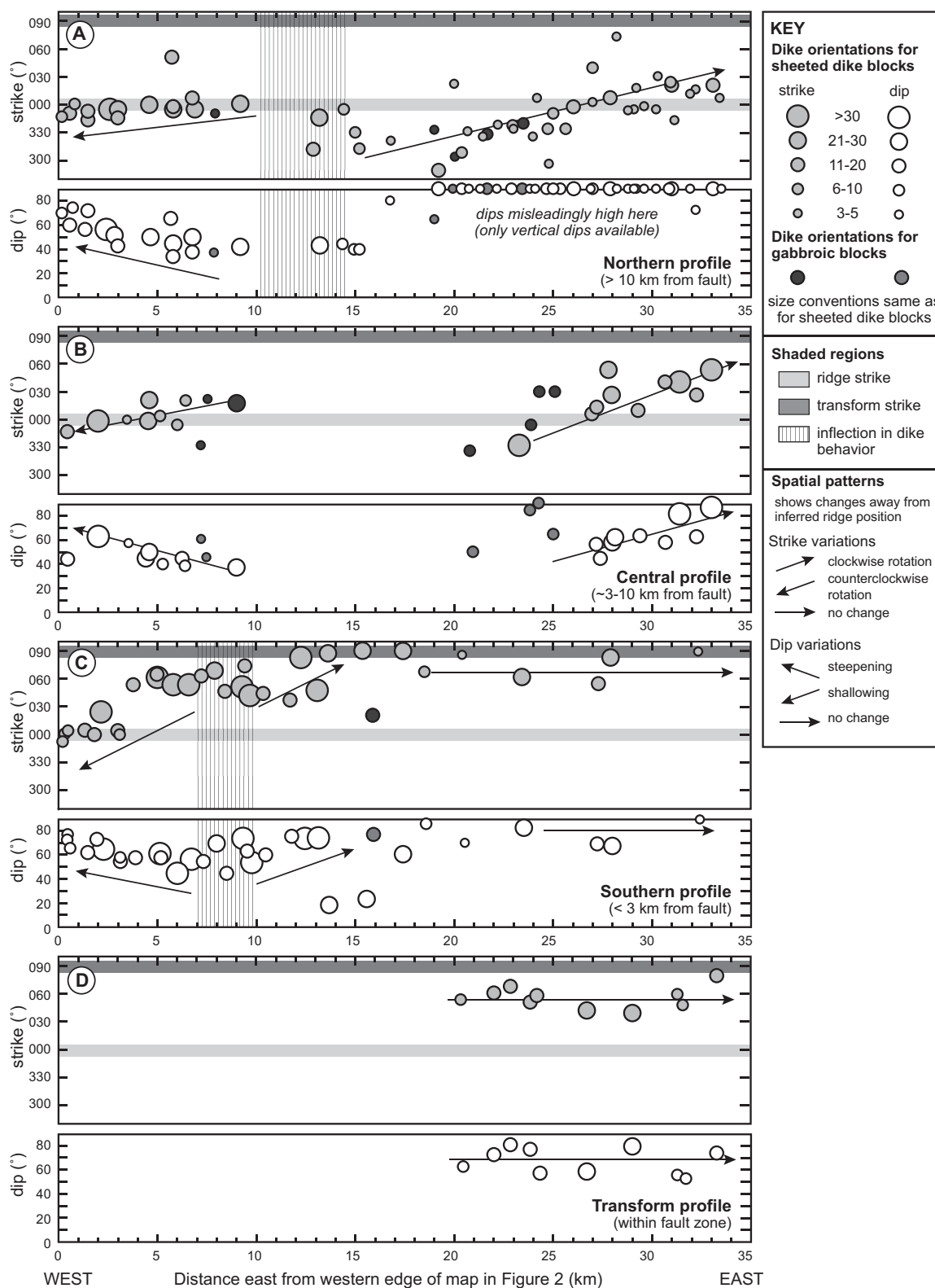


Figure 4. Transect-style summary of dike orientation variations across the study area. Each data point represents the average orientation for a single block; the size of the point reflects the number of measurements that were included to find the average. See Figure 3 for transect boundaries.

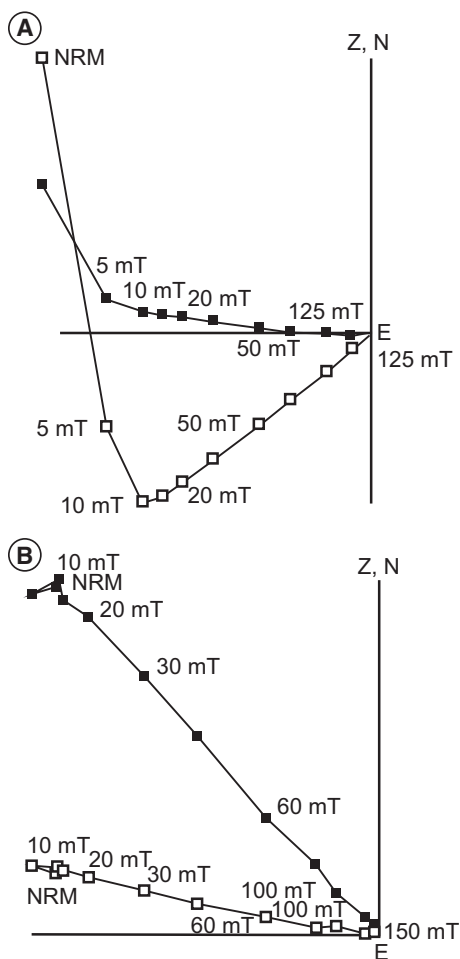


Figure 5. Two representative Zijderveld plots from alternating field demagnetization experiments for samples (A) 38b1b and (B) 52a2a. Closed squares show declination, and open squares show inclination. Both specimens show a secondary magnetic component in the 0–10 mT demagnetization steps. NRM—natural remanent magnetization.

whereas the declination values vary systematically with position. This pattern indicates that most deformation in this region was accommodated by rotation about steeply plunging axes.

NUMERICAL KINEMATIC MODEL

We construct a two-dimensional, numerical kinematic model for deformation within the inside corner of Cyprus. In brief, our model uses paleomagnetic data and present-day (i.e., final) dike orientations to predict initial dike orientations. Integrating the paleomagnetic and dike data sets presents several challenges, each of which may be overcome in multiple ways. To give the reader a sense of the entire process, we first describe the four main steps in our model

TABLE 1. PALEOMAGNETIC RESULTS

Station	Latitude (°N)	Longitude (°E)	N/N ₀	D (°)	I (°)	α95	K	R
33	34°53.641	32°52.144	6/6	229	31	6.2	97	6
36	34°53.591	32°53.906	6/6	263	-32	5.1	147	5
38	34°52.802	32°54.378	6/7	316	-14	9.7	40	5.9
39	34°52.934	32°55.613	5/5	307	10	9.7	51	4.9
46	34°56.580	32°58.219	6/6	256	0	21.4	9	5.5
47	34°56.585	32°59.977	6/6	276	50	6.5	90	6
48	34°55.502	33°00.868	6/6	320	-34	6.8	82	5.9
49	34°52.123	33°04.174	4/6	233	68	2.8	819	4
50	34°53.720	33°00.900	6/6	327	53	13.3	20	5.8
51	34°55.405	32°58.328	6/6	327	47	12.9	23	5.8
52	34°54.418	32°59.499	5/5	281	37	4.3	255	5
53	34°54.493	33°00.355	4/6	118	21	17.2	22	3.9
55	34°53.122	32°57.005	6/6	332	19	13.6	6	6
72	34°54.856	33°02.040	6/6	287	26	3.3	343	6
96	34°54.357	32°50.791	6/6	280	85	12.8	24	5.8
122	34°51.016	33°09.627	6/6	57	21	5.2	142	6
131	34°53.801	32°56.148	6/6	290	8	1.8	1210	6
132	34°54.870	32°56.413	6/6	280	28	3.7	280	6
133	34°56.589	32°56.226	5/5	279	30	10	48	4.9
138*	34°51.784	33°02.746	5/5	96	63	13.2	28	5.9
141	34°54.479	33°01.351	5/6	303	11	6.2	121	5
143	34°53.054	32°52.488	6/6	305	10	8.3	55	5.9
149	34°58.485	32°56.876	5/5	244	44	10.4	44	4.9
150	34°57.645	32°55.950	6/6	288	63	7.7	64	5.9

Note: Summary of paleomagnetic data including the number of reliable specimens per station (N/N₀), declination (D), inclination (I), Fisherian 95% confidence interval (α95), precision parameter (K), and the length of the resultant vector of summed direction cosines (R).

using one set of choices, illustrated graphically by the flowchart in Figure 7. Next, we describe how alternative choices for each model step (also shown in Fig. 7), based on geologically reasonable interpretations, affect our predictions of the initial dike strike results.

First Model

First, we define the model coordinate system by assuming that the ridge is straight and N-S-striking, and that the transform is straight and E-W-striking (Fig. 7). By projecting the Solea graben southward from its well-defined field location (Varga and Moores, 1985), we find that the graben intersects the Arakapas fault south of the town of Moniatis (Fig. 2). We impose a coordinate system in which the x-axis coincides with the Arakapas fault and the y-axis coincides with the Solea graben.

Second, we determine the deformation recorded by paleomagnetic data. Because our model is two-dimensional, we are interested solely in the vertical-axis rotation component. We compute the average remanent magnetization direction for groups of nearby stations (Table 2) to smooth the variation from the station-by-station results. For each group, the vertical-axis rotation is determined by comparing the group’s average declination to that of the Troodos mean vector, ignoring the inclination values (Fig. 8). Because

most paleomagnetic inclinations from the inside corner cluster about the Troodos mean inclination (Fig. 6), this is a reasonable first approximation.

At this point, several group means are excluded from our model (see Table 2; Fig. 8). Two sites are not located within the inside corner (12 and 14). Two sites exhibit counterclockwise rotations, which are unexpected in a dextral system and cannot be accounted for in our simple kinematic model (9 and 13). Last, two sites located near the model boundary (i.e., the Arakapas fault) have large clockwise rotations (19 and 20). These rotations exert undue influence on the model results, especially since the rotation at site 19 appears to be anomalously large compared to the regional trend.

Third, we calculate a field of rotations that best matches the paleomagnetic group means throughout the inside corner, in order to characterize deformation at the noncoincident dike sites. We interpolate the vertical-axis rotations, ω, using a function of the form

$$\omega = \omega(x, y) = a x e^{-b y} \tag{1}$$

The fact that ω is proportional to the distance x from the ridge reflects our assumption of a constant spreading rate, captured by the parameter a. The fact that ω is decreasing in y reflects our expectation that more deformation, and hence more rotation, has occurred near the transform

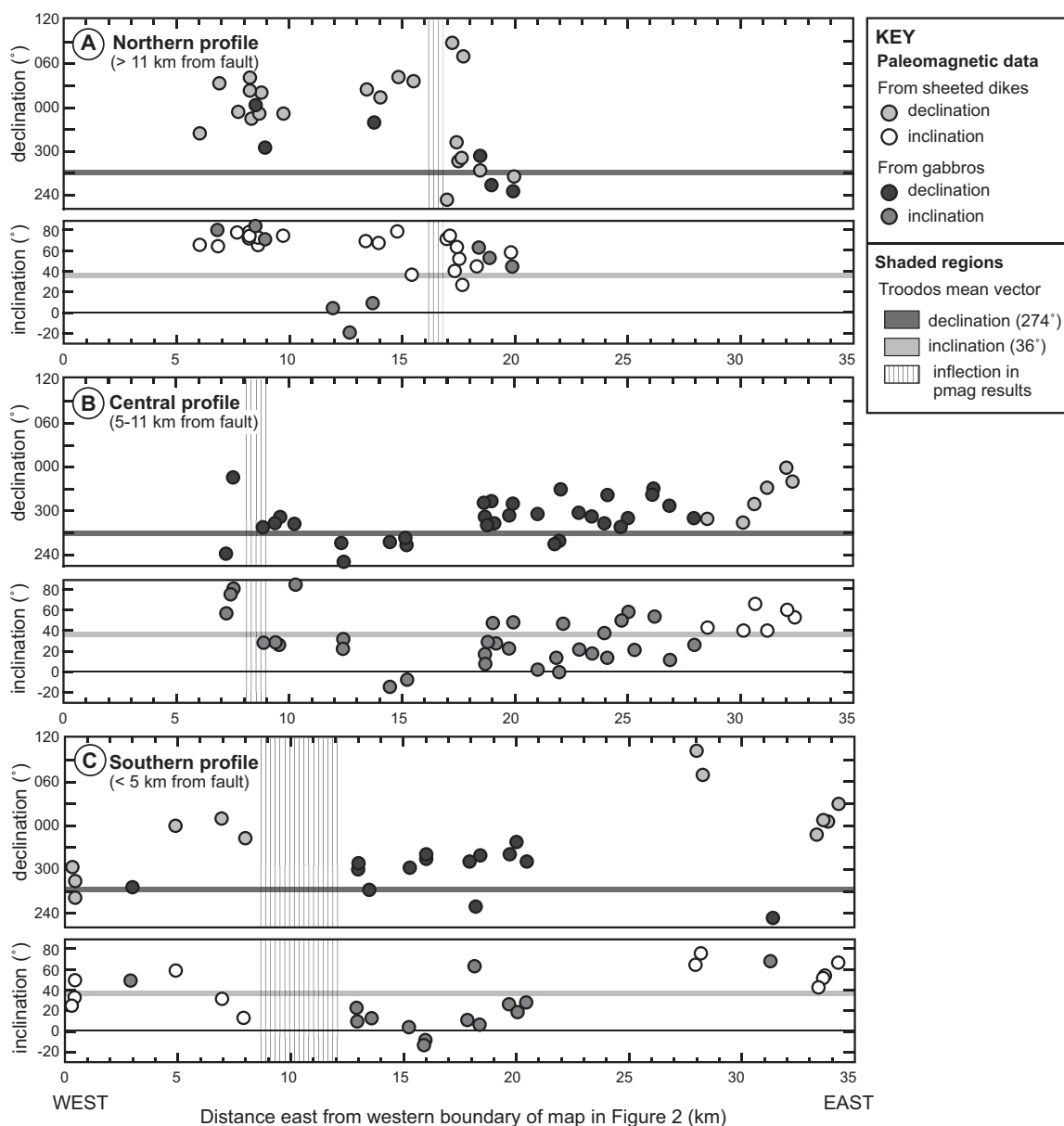


Figure 6. Transect-style summary of paleomagnetic data from Figure 2, with in situ declination and inclination components. The values from the Troodos mean vector are also plotted. For declination plots, values above the mean suggest clockwise rotations. Note: 11 data points plotted in A, compiled from Hurst et al. (1992), are north of the map region in Figure 2.

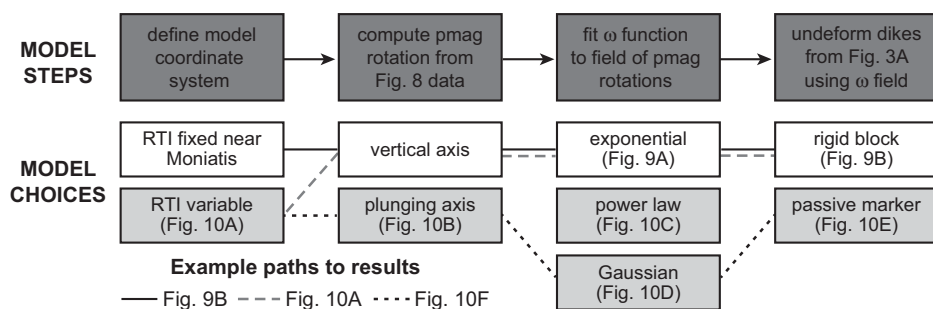


Figure 7. Flow chart illustrating our numerical kinematic model. The dark-gray boxes show the major steps in the model process. The boxes beneath them show choices for each step: White boxes are described in the first description of our model, and light-gray boxes denote alternatives. To produce results showing the initial orientation of sheeted dikes (i.e., Figs. 9B and 10), one choice from each column must be selected. The dotted lines connecting various choices show example pathways that lead to particular results described in the text. RTI—ridge-transform intersection.

TABLE 2. PALEOMAGNETIC GROUP MEANS AND ROTATIONS

Group	Rock type	N per group	D (°)	I (°)	Rotational component			Incorporated in model
					Vertical axis	Plunging N-S axis	Difference	
1	Gabbro	4	302.6	7	29	32	3	Yes
2	Gabbro	3	261.9	-9.13	-12	-12	0	Yes
3	Gabbro	3	303.1	8.4	29	32	3	Yes
4	Gabbro	6	310.3	23.9	36	39	3	Yes
5	Gabbro	2	302.1	26.6	28	30	2	Yes
6	Gabbro	2	309	35.1	35	35	0	Yes
7	Gabbro	3	296.8	12.7	23	26	3	Yes
8	Gabbro	2	281.6	46.1	8	6	-1	Yes
9	Gabbro	2	246.7	49.1	-27	-25	2	No
10	Gabbro	4	307.2	15.3	33	36	3	Yes
11	Gabbro	2	281.5	53.7	8	5	-3	Yes
12	Gabbro	4	281.5	40.8	8	6	-2	No
13	Gabbro	2	242.3	27.1	-32	-31	0	No
14	Gabbro	4	12.3	12.1	98	108	10	No
15	Dike	3	290	50	16	12	-4	Yes
16	Dike	2	345	56.4	71	52	-19	Yes
17	Dike	1	329	40	55	53	-2	Yes
18	Dike	3	353	50.3	79	65	-14	Yes
19	Dike	2	70	39	156	135	-21	No
20	Dike	1	28	67	114	44	-70	No
21	Dike	3	266	62	-8	-8	0	Yes

Note: Summary of paleomagnetic groups, including number of sites per group (N), declination (D), inclination (I), and the vertical-axis rotation component for different treatments for the paleomagnetic results. See text for discussion of outliers rejected from our modeling. Figure 8 also shows the group mean declinations in map view.

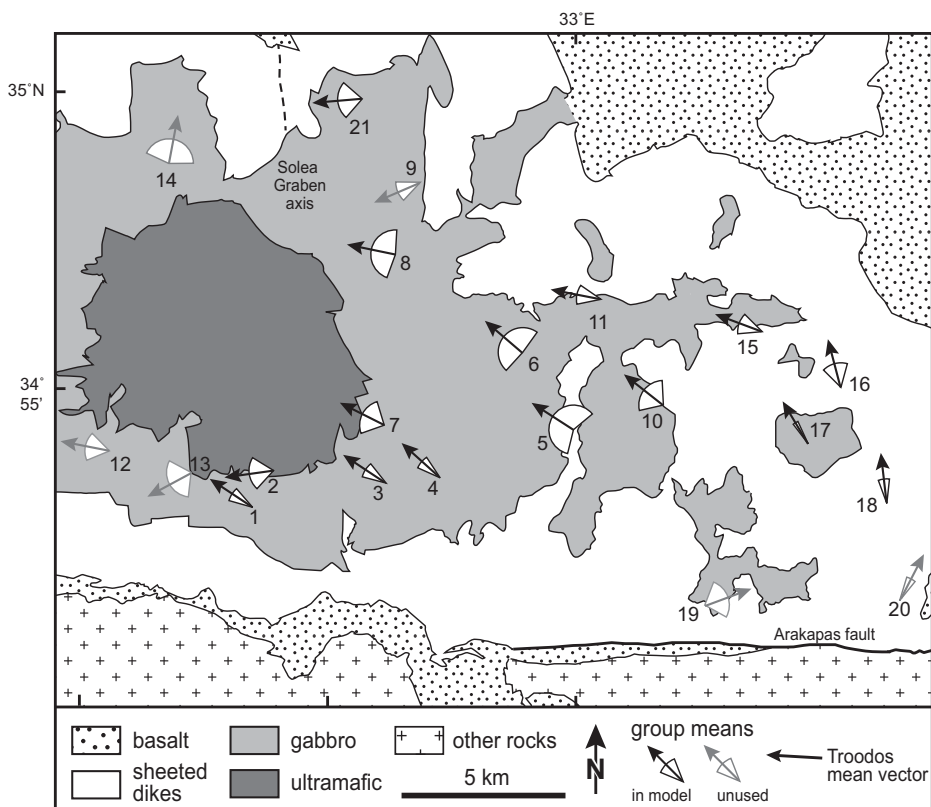


Figure 8. Map showing declination directions from paleomagnetic groups used in our modeling process. Group site numbers correspond to the results presented in Table 2.

fault than far from it. In particular, we employ exponential decay because that kind of decay has been used to model deformation near other large transform faults, such as the Alpine fault in New Zealand (Hall et al., 2004; Rahl et al., 2011). The parameter *b* controls the rate of the decay. We define the misfit between ω and the vertical-axis rotation data in a least-squares sense, giving each datum equal weight.

Using *Mathematica*, we compute values for *a* and *b* that minimize this misfit (Table 3). Figure 9A shows the agreement between the vertical-axis rotations and the best-fit interpolation function. In general, the model is broadly consistent with the observations. The average misfit between the observed and modeled rotations is ~12°. Misfits tend to be largest near the ridge-transform intersection.

The fourth and final step in our model is to unrotate the dikes to determine their initial orientation. In all our models, we assume that dikes initially intruded at the ridge. In this version of the model, we assume that they exist within rigid blocks that rotated independently during steady deformation. For convenience, we use the block boundaries and average dike orientations shown in Figure 3A, although we do not claim that these are the actual blocks that may have rotated. For each dike site, we use the interpolation function ω to compute its rotation, and then subtract this value from the present dike strike. Our method implicitly assumes that although deformation was heterogeneous on the regional scale, it can be modeled as approximately homogeneous on the scale of the crustal blocks. We ignore any potential space problems caused by blocks overlapping or separating during rotation.

The choices described here, and illustrated by the solid black pathway through the white boxes in Figure 7, lead us to our ultimate goal—prediction of the initial dike strikes shown in Figure 9B. Each dike is plotted in its present-day position, but it is important to remember that dikes likely intruded at or near the ridge. Thus, we would expect to see consistent initial dike strikes along a given E-W transect if deformation were steady. Our results suggest that immediately north of the transform fault, dikes have scattered initial strikes with no apparent consistency except locally. Between ~4 and 14 km north of the transform, dikes strikes are consistently NW- or NNW-striking. Farther than 14 km north of the fault, dikes on the west side are also NW-striking, while those on the east are closer to N-S-striking.

Varying the Coordinate System

The ideal model coordinate system is not obvious in Cyprus, because there are several

TABLE 3. KINEMATIC MODEL DETAILS

Model type	$\omega(x, y)$	Error
Simple	$-0.14 x e^{-0.15y}$	0.92
Coordinate system: vary ridge position	$-0.12 (x + 3.1) e^{-0.16y}$	0.87
Vertical-axis rotation: plunging axis	$-0.13 x e^{-0.14y}$	0.97
Vorticity field interpolation: power function	$-0.28 x y^{-0.89}$	0.96
Vorticity field interpolation: Gaussian function	$-0.09 x e^{-(y^2/90.2)}$	0.89
Combined choices	$-0.06 (x + 6.1) e^{-y^2/80.3}$	0.78

Note: Summary of modeling results including the best-fit equation for the vorticity function ω and the associated least squares error. Note that x and y have units of kilometers.

competing hypotheses about the location of the Solea graben axis in the literature. All workers seem to agree on the northern portion of the graben, the approximately N-S-striking segment constrained by field observations of inwardly dipping dikes toward a central axis (Varga and Moores, 1985; Varga, 1991; Hurst et al., 1994). From this location, Abelson et al. (2002) extended the ridge axis toward the east, meeting the Arakapas fault near the town of Kalocho-rio (Fig. 2). This intersection creates an obtuse angle between the two structures within the inside corner. Alternatively, the Open University

group (MacLeod et al., 1990; Gass et al., 1994) proposed that the ridge-transform location was near the town of Mandria, resulting in a slightly acute angle for the inside corner.

Every model presented in this paper assumes an orthogonal ridge-transform intersection. Initial modeling using acute and obtuse angles suggested that our data sets are not rich or detailed enough to constrain the angle of intersection. We do, however, allow the ridge-transform intersection to translate east and west, to explore the effect of ridge position. Keeping all other model choices the same as in the initial model

(see the gray pathway in Fig. 7), we find that the best-fit location is ~3 km west of our initial location, toward the prediction of MacLeod et al. (1990). This shift effectively means that all dike locations are farther from the ridge than in our first version of the model.

Figure 10A shows the predicted dike strikes based on this new location of the ridge-transform intersection. The contours in this panel (and all others in Fig. 10) represent the difference in dike strikes between the new model and the first model (Fig. 9B). The effect of moving the ridge is greatest near the ridge-transform intersection, as indicated by increasing contour lines toward the SW. For the rest of the region, dike strikes are fairly similar between the two models. This consistency is quantitatively described by computing the average angular difference between these results and those from Figure 9B, which is $7.0^\circ \pm 0.5^\circ$.

Alternative Computation of Vertical-Axis Rotations

Most of the paleomagnetic data in the inside corner come from sites located within the gabbros.

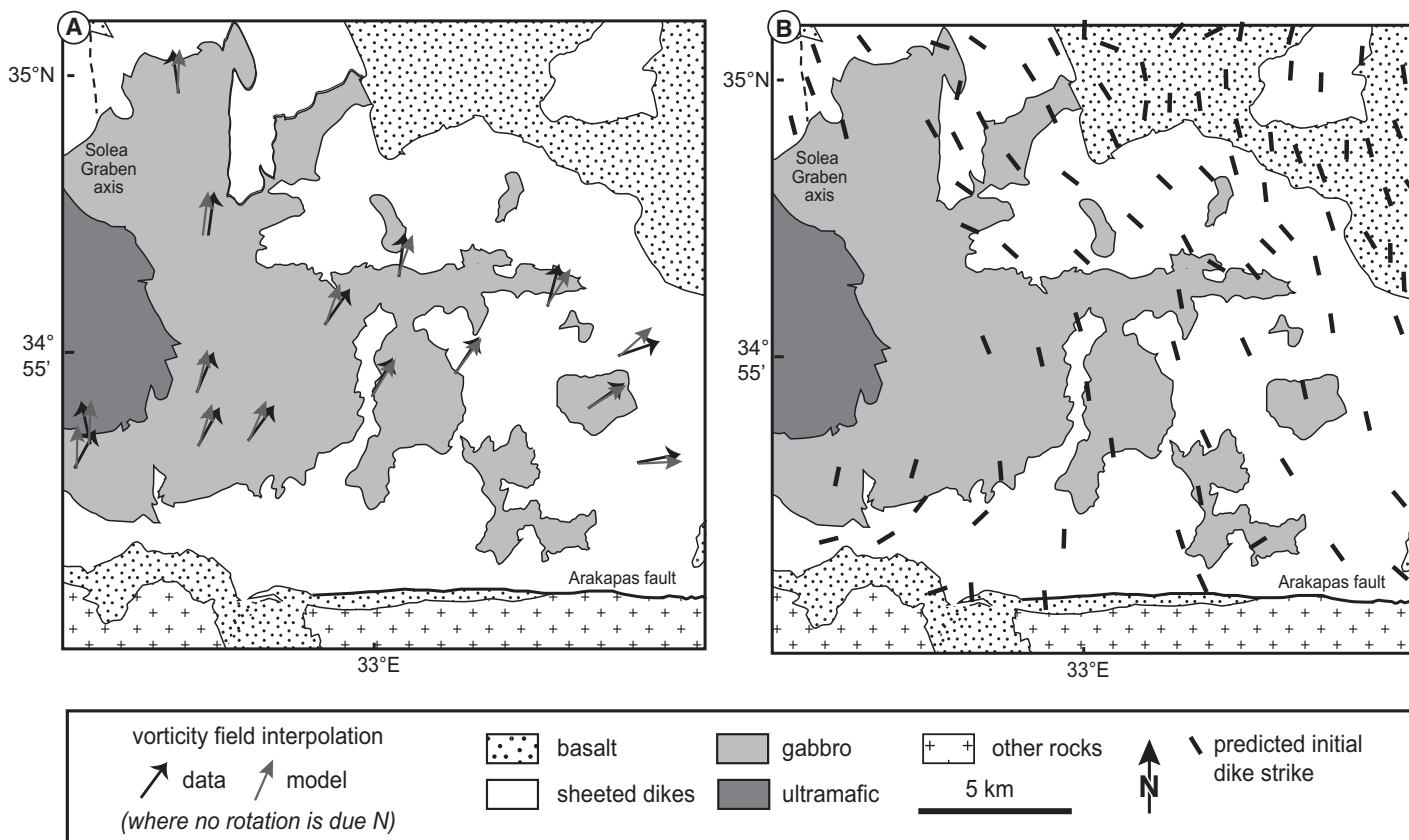


Figure 9. Results from our first description of modeling choices. (A) The fit of our vorticity field ω to the vertical-axis rotation data using the exponential function from Equation 1. Each arrow indicates the magnitude of vertical-axis rotation, where a N-directed arrow denotes no vertical-axis rotation. (B) The predicted initial sheeted dike orientations from this vorticity field, assuming dikes are part of rigid blocks.

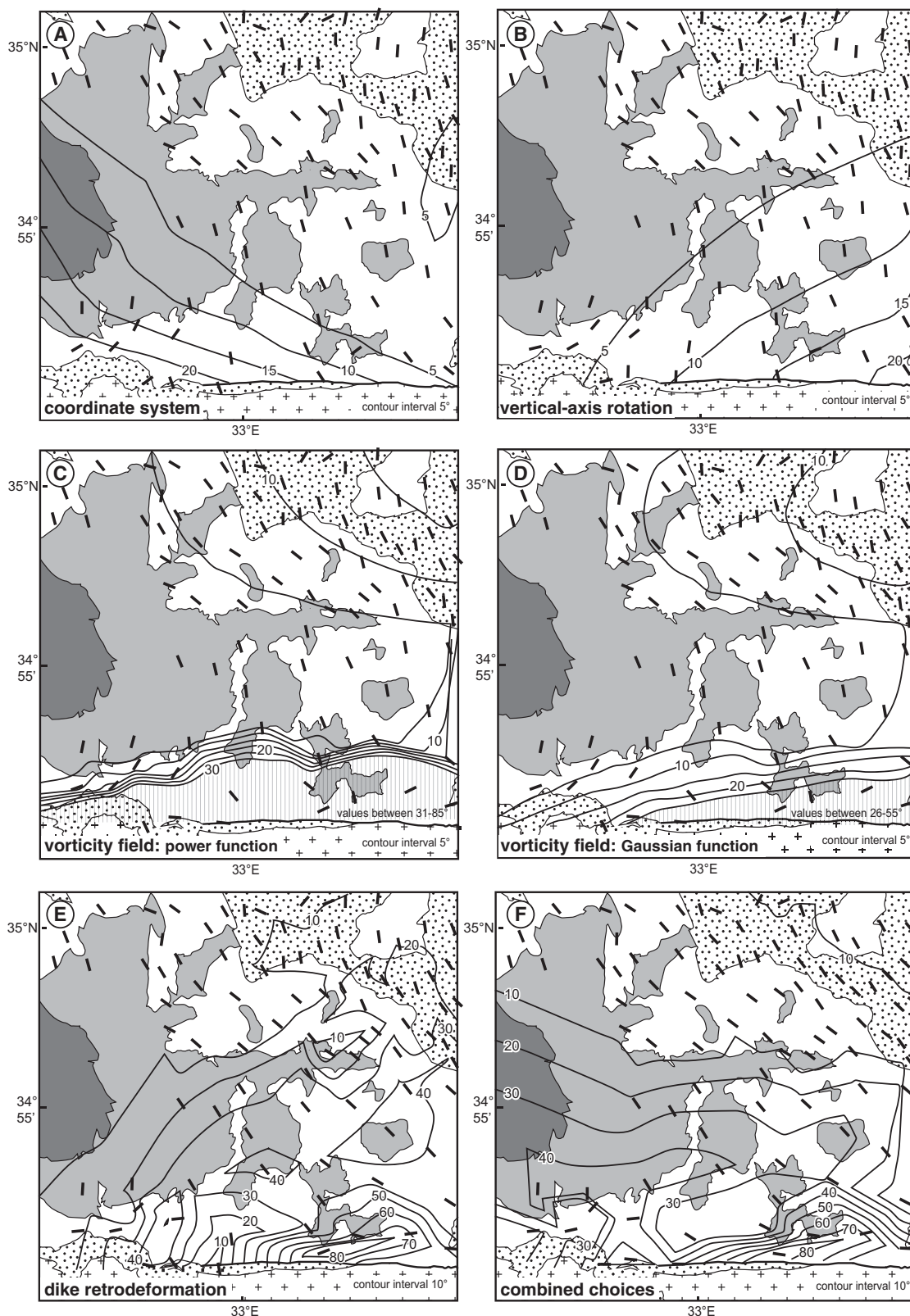


Figure 10. Initial sheeted dike strikes based on alternatives for our modeling choices including (A) relaxing the ridge position, (B) determining the component of vertical-axis rotation from plunging axis rotations, (C) using a power function to fit the vorticity field, (D) using a Gaussian function to fit the vorticity field, and (E) treating dikes as passive markers during retrodeformation. (F) Illustrates the best-fit combined solution that is described in the text. In each panel, contours indicate the difference of the modeled dike strike to the results shown in Figure 9B. Map units and scale are the same as those in Figure 9.

Since these rocks contain no paleohorizontal or paleovertical indicators, it is impossible to determine rotations uniquely without making assumptions about the rotation axis or magnitude. In our first model, we ignored inclination values altogether and assumed a strictly vertical axis for rotation. To incorporate both inclination and declination information, we follow the approach of Abelson et al. (2002) by assuming that rotations occurred about plunging axes parallel to the ridge (i.e., N-S-trending). For each paleomagnetic group, we determine the smallest rotation R , among all rotations about a N-S-trending axis, that takes the observed paleomagnetic vector to the Troodos mean vector. We then determine the vertical-axis component of R by computing the (2, 1) entry of the infinitesimal rotation $\log R$ (Davis and Titus, 2011).

For each paleomagnetic group, the vertical-axis rotation produced by this method deviates less than 3° from the result of the earlier, simpler method (Table 2). (Larger deviations were produced at some sites, such as groups 19 and 20, but these were already excluded from our modeling as outliers.) Given this small difference in vertical-axis rotation values, there is little change to dike strikes for most of the inside corner (Fig. 10B). The largest change is found in the SE corner, where no paleomagnetic data constrain the modeling. The average difference between these model results and those of the simple model is $5.9^\circ \pm 0.3^\circ$, which is the smallest effect of any alternative modeling choice that we tested.

Alternative Interpolation Functions

In the first version of our model, we used an exponential function e^{-by} to model decreasing rotation away from the transform fault. Here, we test two alternatives: the power function y^{-b} and the Gaussian function $e^{-y^2/b}$. In each case, the parameter b controls the rate of decrease. These functions differ from the exponential function markedly in the region near the transform fault, where the exponential function had more difficulty in fitting the data (Fig. 9A).

Using a power function to fit paleomagnetic rotations affects dike strikes in two regions (Fig. 10C). Those dikes in the NE are mildly altered, with strike changes up to 15° . Because the power function has an asymptote along the transform fault, dikes along the fault are greatly affected, with differences at individual stations as large as 85° . In the central corridor, the dike strikes are quite similar to those from the original model (Fig. 9B). The average angular change is $24.4^\circ \pm 8.5^\circ$ throughout the inside corner.

The Gaussian function produces results that are similar in appearance to the power function

(Fig. 10D). Dike strikes vary most in the NE and along the transform fault. However, the variations near the transform reach maximum values of only 55° , resulting in a smaller average angular change of $12.4^\circ \pm 1.3^\circ$.

Rigid versus Passive Dike Rotation

Our first approach to retrodeformation assumed that dikes were part of rigid blocks rotating adjacent to the Arakapas fault, a common interpretation in transcurent environments (e.g., Ron et al., 1984). An alternative interpretation of the paleomagnetic rotations, and therefore the dike retrodeformation, is based on a continuum approach (e.g., Sonder et al., 1986; Lamb, 1987). Continuum models may be appropriate when the block size is small relative to the overall size of the deforming zone, and when deformation increases with proximity to the major fault (Sonder et al., 1994). Both of these conditions hold in Cyprus.

To quantify the passive rotation of dikes, we must develop a finite deformation (or velocity) field from our field of vertical-axis paleomagnetic rotations. As before, we assume that the deformation is steady in time and locally homogeneous. Because a vertical-axis rotation amounts to one scalar datum at each dike site, we have just one degree of freedom in selecting the homogeneous deformation at each site. So we assume that the deformation is steady simple shearing along the transform fault. The position gradient tensor F is

$$F = F(x, y) = \begin{bmatrix} 1 & \gamma(x, y) \\ 0 & 1 \end{bmatrix}.$$

Here, $\gamma = \gamma(x, y)$ is the shear strain, which relates to vertical-axis rotation ω by $\gamma = -2\omega$ (McKenzie and Jackson, 1983). In detail, at each dike site, we use the interpolated ω to find F , and then we use F^{-1} to retrodeform the observed dike orientation back to a predicted initial orientation.

What is most notable about our passive treatment of dikes is the consistent NW strike for dikes, observed everywhere except the 5 km band north of the transform fault (Fig. 10E). This modeling choice produced an average angular change of $25.5^\circ \pm 5.3^\circ$ relative to the first model—the largest difference of any of the alternative modeling choices. In detail, however, the angular change in dike strike is quite small for most of the region. The major difference occurs in the SE corner where the largest rotations are expected, and this is caused by the different conceptual models for dike rotation. When dikes rotate as part of rigid blocks, as in

our first version of the model, they can rotate indefinitely at high strains. In contrast, when they are treated as passive markers, they cannot rotate past the strike of the transform fault.

All Variations Combined

We conclude with a single model that combines four of the modeling alternatives just described: varying the ridge location, vertical-axis rotations computed from plunging axis rotations, a Gaussian interpolation function, and passive rotation of dikes. This set of choices is illustrated by the black dotted pathway on Figure 7.

In the best-fit model (Table 3), the ridge shifts 6 km westward. Transform-parallel dikes are predicted adjacent to the fault, with consistently NW-striking dikes at distances of 4 km or more from the fault (Fig. 10F). The predictions differ markedly from the first model's predictions (Fig. 9B) near the transform fault. This discrepancy is primarily due to the change in interpolation function (Fig. 10D) and the passive, rather than rigid, dike rotation (Fig. 10E).

Comparison of Modeling Results

Although the details of our results vary depending on our specific modeling choices, all of our models exhibit a few broad patterns (Figs. 9 and 10). We discuss these patterns along three E-W-oriented transects that coincide with those from the paleomagnetic data set (Fig. 6).

For the northern transect, dikes typically change from NW-striking on the west side to N-S-striking on the east side. We believe the NW strikes on the west are reliable. No appreciable declination variations exist in this region (Fig. 6A), and NW-striking dikes were one of two solutions that matched local paleomagnetic studies (Allerton and Vine, 1987; Hurst et al., 1992). In contrast, the results from the east side can be discounted for two reasons. First, the field of rotations is not constrained by paleomagnetic data. Second, the eastern rocks are primarily basalts, located stratigraphically above the sheeted dike complex. These rocks may not have recorded the same deformation history as deeper lithospheric units.

Our model results are most consistent along the central transect, both within each model and among different models. In all variations, dikes are predicted to strike NW or NNW along the entire transect. Our paleomagnetic data set is richest along this transect and seems to be least affected by inclination variations (Fig. 6B), making it easier to isolate the vertical-axis rotation signal and to constrain the field of rotations.

For the southern transect, the predicted dike strikes vary both among models and within a

single model. This transect has a better set of paleomagnetic data than the northern transect (Fig. 6C), so lack of paleomagnetic data may not be the cause of the inconsistencies. Instead, the assumption that all dikes along the transect originally intruded at the ridge may be overly simplistic. Field observations clearly indicate that there are multiple generations of dikes north of the Arakapas fault (e.g., Gass et al., 1994). If we knew which dikes in Figure 2 belonged to the earliest generation, we might have more consistent model results along this transect. However, culling the dike orientation data is not presently possible without more detailed field observations north of the Arakapas fault.

DISCUSSION

We do not suggest that the dike strikes from our modeling results should be interpreted as the exact initial orientation of dikes. Yet the consistent NW strikes observed for the best-constrained central transect in all versions of our results (Fig. 10) are quite different from the classic interpretation that dikes began as N-S–striking features (Simonian and Gass, 1978). This NW orientation could result from at least three different scenarios.

Ridge Orientation

One possibility is that the ridge itself was NW-striking and that dikes initially intruded parallel to the ridge. This orientation is consistent with the ridge axis proposed by Abelson et al. (2001, 2002), who used anisotropy of magnetic susceptibility data to suggest an eastward swing of the ridge axis into a NW-striking orientation (Fig. 11).

In this scenario, dikes on both sides of the ridge would presumably intrude with NW strikes. However, those on the west side are consistently N-S– or even NE-striking (Fig. 11A), with little evidence for vertical-axis rotation (Fig. 11C). Thus, there is no mechanism for the dikes to change their orientations. Paleomagnetic data on the east side are also inconsistent with a NW-striking ridge, at least in its proposed location. Many of the sites with large clockwise rotations would be located on the outside (non-plate boundary) corner of the system, where clockwise rotations would be unexpected (Fig. 11C).

Instead of a NW-striking ridge segment, we suggest that the ridge location may be better constrained by the inflection points from our transect-style analysis of dikes and paleomagnetic data. These inflections are not perfectly consistent between data sets (Fig. 11), but they do suggest a general N-S strike for

the ridge, essentially along the western edge of the ultramafic exposures. At the very least, the ridge strike is unlikely to be parallel to the predicted initial NW-striking dikes from our model results.

Detachment Fault

A second possibility is that the NW strike of dikes is an artifact of our model construction, which combined field data from different crustal levels. Sheeted dikes and gabbros could have been decoupled during deformation by a midcrustal detachment fault, which are common structures near modern ridge-transform intersections (e.g., Karson, 1999; MacLeod et al., 2002; Smith et al., 2008). A fault placing gabbroic rocks in the footwall of the system and sheeted dikes in the hanging wall would cause these rocks to experience different deformation histories (Fig. 11B). In Cyprus, several studies have documented and/or suggested the presence of a detachment fault, making this an important consideration for interpreting our model results.

Several workers (Varga, 1991; Hurst et al., 1994) have mapped the shallowly dipping Kakopetria detachment fault north of the ultramafic exposures (Fig. 11A). Hurst et al. (1994) suggested that the fault is listric, which allowed crustal blocks to tilt about ridge-parallel axes (Fig. 11B). Although this fault is outside our model region of interest, it is the only example of a detachment fault in Cyprus where field mapping was used to constrain the fault geometry.

Nuriel et al. (2009) used oxygen isotopes in serpentinites to argue that an oceanic detachment fault—the Amiandos fault—facilitated exhumation of the ultramafic rocks in the Troodos ophiolite (Fig. 11B). This fault is NW-striking, located along the eastern contact of the ultramafic rocks, and vertical or steeply NE-dipping. The steep dip of the Amiandos fault effectively limits the extent to which this fault could have decoupled sheeted dikes and gabbros in the main model region.

Granot et al. (2006) suggested the presence of a detachment fault between crustal levels north of the Arakapas fault, which poses the largest concern for our model results. This idea stems from comparisons of sheeted dike strikes and paleomagnetic data from gabbros. By assuming dikes began as N-S–oriented features, their present-day azimuth is used as a measure of total deformation. Granot et al. (2006) found that dike deflection was greater than paleomagnetic declination rotation by $\sim 20^\circ$. However, as discussed previously, not all paleomagnetic models of fault systems indicate that crustal blocks should be treated as rigid (e.g., Sonder et al., 1994). Thus, a one-to-one correspondence

between dike deflection and paleomagnetic data is not required in a deforming zone. Further, instead of assuming a particular initial orientation of dikes, we can simply compare their orientation changes as a function of their position. North of the Arakapas fault, dike strikes change by $\sim 60^\circ$ (from azimuths of 030° to 090° ; Fig. 4C). For the same region, paleomagnetic data show $\sim 60^\circ$ of clockwise rotation (Fig. 6C). Thus, there may be no discrepancy between these data sets. Without more detailed mapping to identify a detachment fault in the field, we believe that this explanation can be rejected as the cause for the NW-striking dikes in our model results.

Heterogeneous Stresses

The third possibility is that the NW initial dike strikes simply reflect the preferred orientation for dike intrusion near the ridge-transform intersection. This idea is supported using insights from dynamic models, such as the five examples shown in Figures 12A–12E. In each panel, we plot the maximum horizontal stress directions. These directions should parallel the initial strike of dikes in map view, thereby facilitating comparisons to our kinematic model results.

Figure 12F represents an attempt to synthesize common findings across dynamic models. Three regions are worth highlighting: (1) For the inside corner, all models predict NW-striking dikes, although the azimuth depends on the specific model parameters such as spreading rate, fault locking, offset length, etc. (2) For the outside corner, all models predict deflection in the opposite, NE-striking sense. For any given model, the amount of this deflection is less than the deflection observed for the inside corner. (3) Along the transform fault, the models differ in their predictions by up to 90° , ranging from fault-parallel to ridge-parallel maximum horizontal stress directions.

In general, dikes in Cyprus are consistent with dynamic model predictions for the inside and outside corners when combined with the independent knowledge of rotations from paleomagnetic data. For the inside corner, we observe NW-striking dikes in our kinematic model results once rotations have been removed. For the outside corner, NE-striking dikes are observed close to the transform fault where paleomagnetic rotations are negligible (Fig. 11), suggesting that these NE strikes are original.

Independent support for these stress-orientation deflections at the inside and outside corners comes from paleostress analysis of slickenside striations on small faults near the Solea graben (Fig. 11C). On the east (inside corner) side of the graben, Hurst et al. (1994)

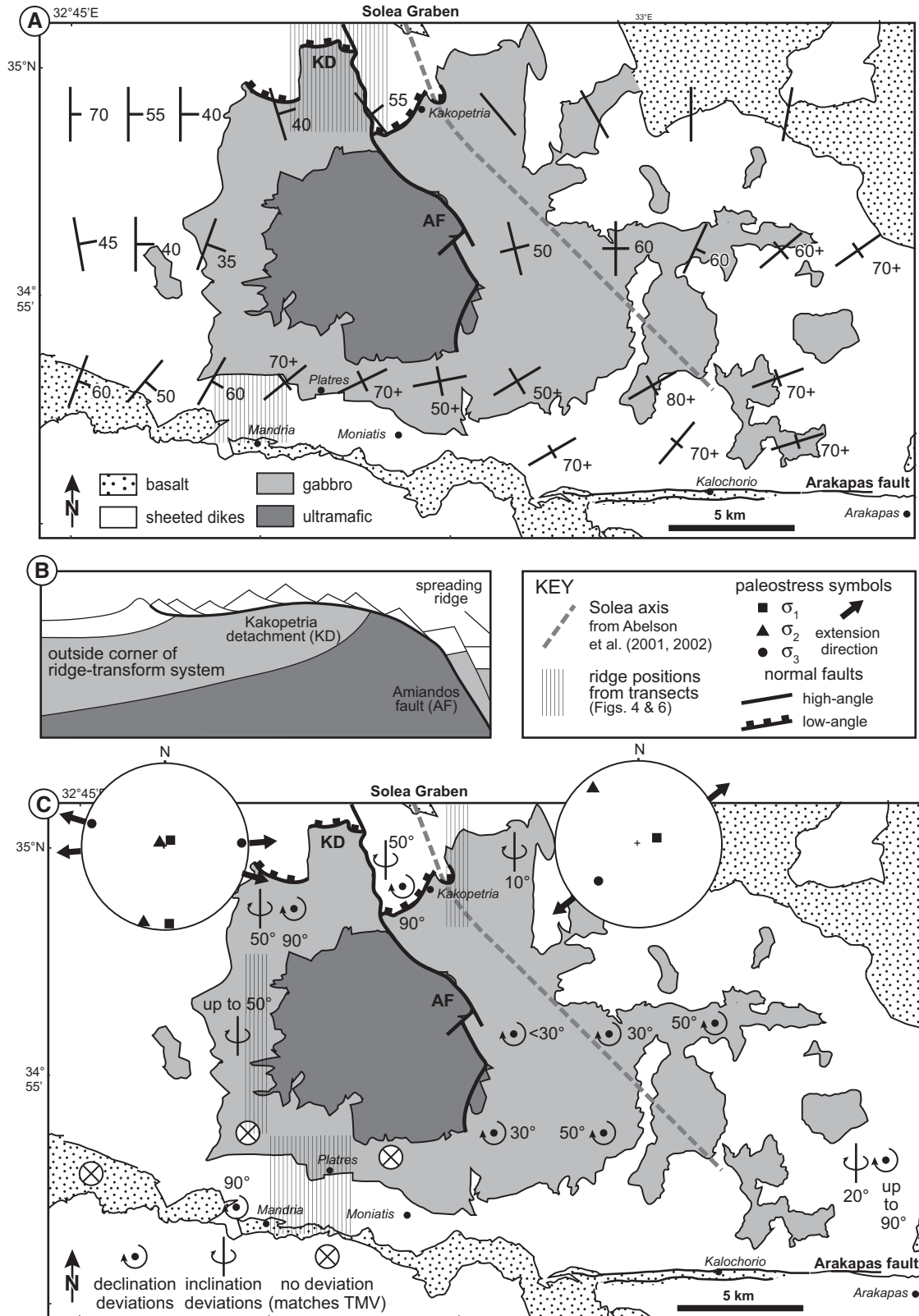


Figure 11. Summary of relevant geologic features for interpreting model results of inside corner deformation. Geologic map units are the same as those in Figure 8. (A) Summary of dike orientations. (B) Cartoon of a detachment fault in an oceanic core complex. The low-angle portion might explain the geometry of the Kakopetria detachment fault (KD); the high-angle portion was proposed for the Amiandos fault (AF). Figure is modified from Nuriel et al. (2009). (C) Summary of paleomagnetic data showing that clockwise block rotations occur on both sides of the Abelson et al. (2001, 2002) Solea axis. Insets show paleostress orientations for the east (Hurst et al., 1994) and west (Varga, 1991) sides of the Solea graben. TMV—Troodos mean vector.

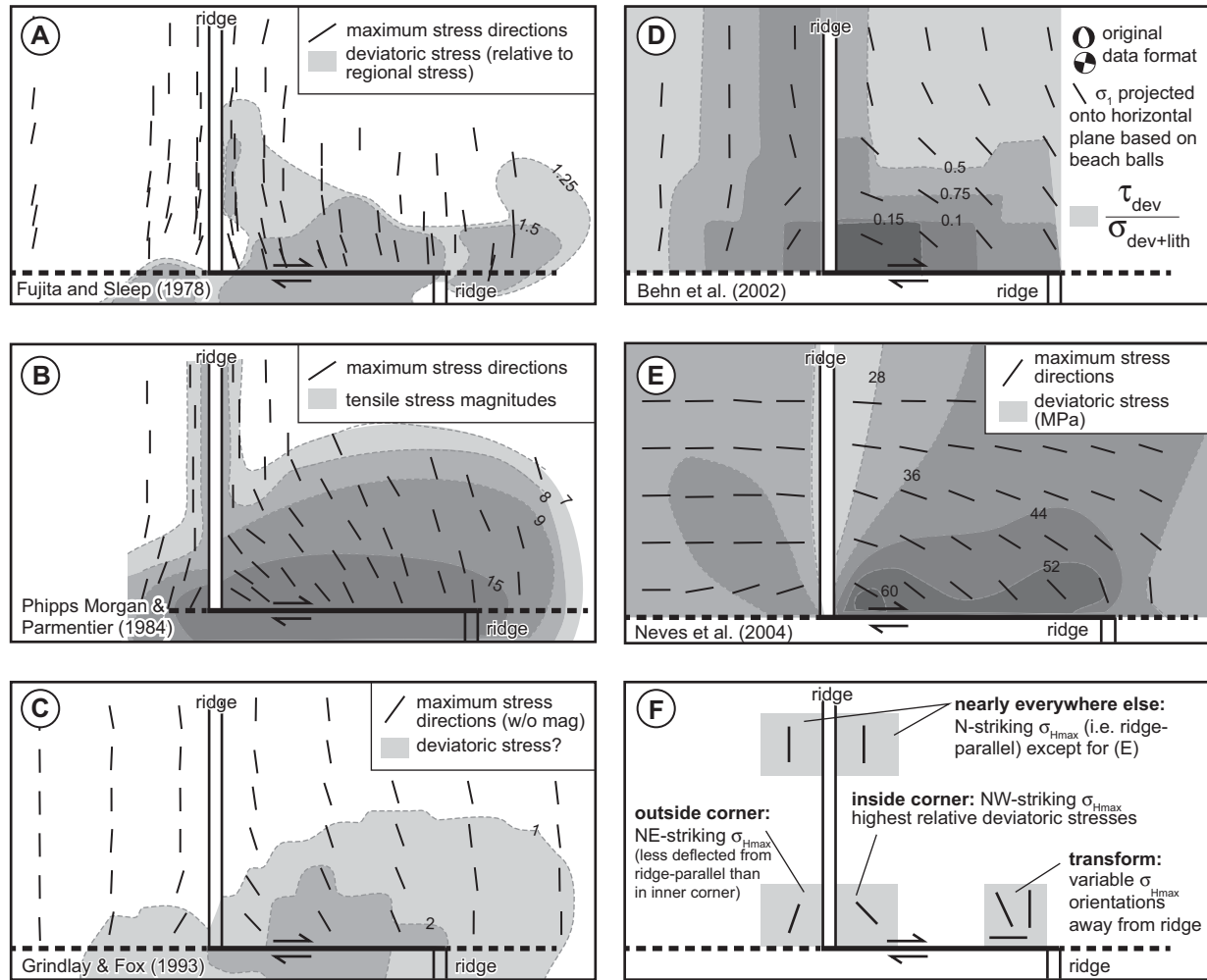


Figure 12. Compilation of dynamic model results for ridge-transform systems. Each diagram may have been altered from its original format by rotation, reflection, or in some cases by plotting the maximum (as opposed to minimum) horizontal stress directions. (A) Model treats the plate boundaries as anisotropic weaknesses in a viscous plate. (B) Model uses a ridge-perpendicular normal stress and a fault-parallel shear stress on transform systems with large offsets (100 km). (C) Model shows the results for a small ridge offset and slow spreading rate. (D) This model is the only example of a boundary-element model, originally presenting three-dimensional stress directions as focal mechanisms. From these, we estimated the orientation of the maximum horizontal stress directions for the purposes of comparison with other studies. (E) Model examined the effect of seafloor subsidence, arguing that ridge-parallel stresses may be larger than ridge-perpendicular stresses due to topographic differences. (F) Here, we synthesize common observations across these different model results. The maximum horizontal stress direction is denoted σ_{Hmax} .

determined stress directions consistent with NW-striking dikes. On the west (outside corner) side of the graben, Varga (1991) found stress directions that would promote intrusion of N-S- or NNE-striking dikes.

In the third important region, near the transform fault, our kinematic model was unable to produce consistent dike orientations within a single model or across models (Fig. 10). Different dynamic models also predict wildly varying stress directions near the transform fault. Thus, deformation may be too complex near the transform fault to be adequately matched by simple models, either kinematic or dynamic in their construction.

Implications

This study highlights the difficulty of comparing the results from dynamic models to field data collected from natural ridge-transform systems. This type of comparison is critical, however, since strict interpretations from either perspective cannot fully explain patterns of inside corner deformation. Using the example from Cyprus, application of the dynamic modeling viewpoint to the curvature of dikes erroneously indicated that the Arakapas fault was sinistral (e.g., Varga and Moores, 1985). However, the classic kinematic interpretation for the same field data (e.g., Simonian and Gass,

1978) cannot explain the NW-striking dikes in our model results.

For dynamic models of ridge-transform systems, it is therefore critical to consider more than the instantaneous view of deformation. Consider the different deformation histories of three dikes labeled *a*, *b*, and *c* in Figure 13A. Their initial formation is controlled by stresses near the ridge (first panel). As dike *a*, which is farthest from the transform fault, translates away from the ridge, it experiences no changes in the local stress directions. Thus, this dike will maintain its initial orientation over time (second and third panels). However, dikes *b* and *c* will rotate clockwise due to the changing stress

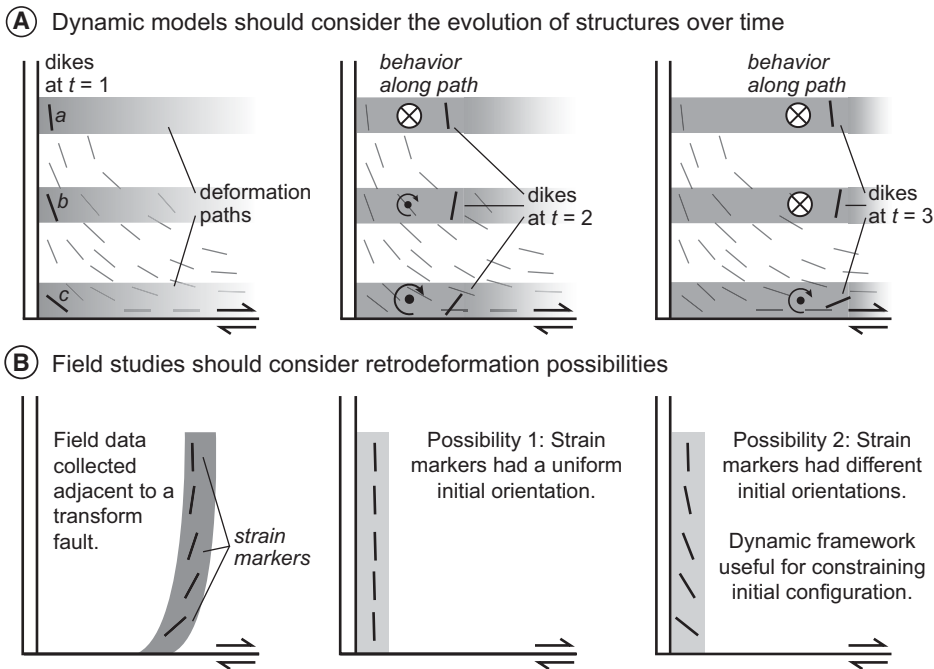


Figure 13. Suggestions for the interpretation of dynamic models of and field data from ridge-transform systems. (A) Three imaginary dikes are tracked through different time steps (t) to illustrate that the heterogeneous stress field can cause varying amounts of rotation. Symbols for rotation are the same as those used in Figure 11. (B) The final state of field data (first panel) could have resulted from numerous initial configurations of strain markers (e.g., second and third panels). Without recognizing the results from dynamic models, it would be tempting to choose the simplest version—uniform orientations—but this may not be appropriate for ridge-transform systems.

directions along their deformation paths. The magnitude and duration of these rotations are different because of the dikes' different starting positions relative to the fault. The point of this simple cartoon is that field features, from fossil or active systems, should not automatically be used to infer stress directions unless they are adjacent to the ridge and have had no time for postemplacement deformation.

For field-based studies, it is important to recognize that individual structures may have experienced different deformation paths to reach their present state. Imagine collecting field data perpendicular to a transform fault, where strain markers showed clear variations with distance from the fault (first panel in Fig. 13B). A common approach would be to assume that each strain marker had the same starting orientation (second panel), analogous to the deflection of foliation by a small-scale shear zone (Fig. 1F). However, a heterogeneous starting configuration is also a viable scenario (third panel). In many cases, the distinction between these two possibilities would be difficult to determine based on field data alone, but the insights from dynamic models suggest that the second option would be more appropriate when the fault is part of a larger ridge-

transform system. Failure to incorporate this information in the interpretation of field data would result in an underestimate of the total strain within an inside corner.

Ultimately, our modeling procedure is rather simple. Nonetheless, it represents a unique, hybrid attempt to quantitatively analyze field data from a ridge-transform system, which may serve as an example for further comparisons between field studies and dynamic models. In the future, we hope to incorporate our own dynamic models for this particular field site. Also, we hope to expand our analysis to three dimensions, since the few dynamic models that report three-dimensional stresses indicate that they are not horizontal for the inside corner (e.g., Behn et al., 2002). The large dike orientation data set from Cyprus has the potential to record patterns of three-dimensional deformation.

CONCLUSIONS

The Troodos ophiolite preserves a well-developed, ridge-transform intersection between the N-S–striking Solea graben and E-W–striking, dextral Arakapas fault. We used two large field data sets—dike orientations and paleomagnetic rotations—compiled from our own mea-

surements and from the literature, to constrain deformation within the inside corner using a numerical kinematic modeling approach. We tested several different versions of the same essential modeling process, where paleomagnetic data were used to create a vorticity field throughout the inside corner, which was then used to undeform sheeted dikes to their presumed initial orientations. In most of our model results, a consistent initial NW strike is observed for sheeted dikes more than 5 km from the transform fault. This NW strike matches predictions of stress directions from dynamic models of ridge-transform intersections, which is our preferred interpretation for the model results.

Our results are significant for both dynamic and field-based approaches to studying deformation within inside corners. From the dynamic model perspective, it is clear that the present orientation of dikes cannot be used to infer paleostress directions without considering how material deforms as it migrates through a heterogeneous stress field. From the field-based perspective, the consistent NW strike is not parallel to the N-S–striking paleoridge. Most previous field studies in Cyprus have assumed that dikes would initiate parallel to the ridge and subsequently rotate due to transform fault deformation. Thus, these studies implicitly underestimate the total deformation. Although our modeling approach is simple and two dimensional, it represents a real step toward linking the results of dynamic models with those of field-based studies in ridge-transform systems.

ACKNOWLEDGMENTS

We thank Mike Jackson and Julie Bowles at the University of Minnesota's Institute of Rock Magnetism for their friendly help and patience. We also thank Zomenia Zomeni from the Cyprus Geological Survey for logistical support in the field. Rachel Walters, Bob Varga, and Ray Russo are thanked for their constructive reviews. This material is based on work supported by an Allensworth fellowship from the Department of Geology at Carleton College (Scott), the Carleton College Class of '49 Fellowship (Titus), and National Science Foundation grants EAR-1151851 and EAR-1119181. Support for writing was provided by a GAIN workshop funded by National Science Foundation grants HRD-0620101 (Mary Anne Holmes) and HRD-0620087 (Suzanne O'Connell).

REFERENCES CITED

- Abelson, M., Baer, G., and Agnon, A., 2001, Evidence from gabbro of the Troodos ophiolite for lateral magma transport along a slow-spreading mid-ocean ridge: *Nature*, v. 409, p. 72–75.
- Abelson, M., Baer, G., and Agnon, A., 2002, Fossil ridge-transform intersection in the Troodos ophiolite: New perspectives from rock magnetism in the gabbro suite and fracture mechanics analysis: *Geochemistry, Geophysics, Geosystems*, v. 3, doi:10.1029/2001GC000245.
- Allerton, S., and Vine, F.J., 1987, Spreading structure of the Troodos ophiolite, Cyprus: Some paleomagnetic constraints: *Geology*, v. 15, p. 593–597, doi:10.1130/0091-7613(1987)15<593:SSOTTO>2.0.CO;2.
- Allerton, S., and Vine, F.J., 1990, Palaeomagnetic and structural studies of the southeastern part of the Troodos complex, in Malpas, J., Moores, E.M., Panayiotou, A., and Xenophontos, C., eds., *Ophiolites, Oceanic Crustal*

- Analogues: Proceedings of the Symposium "Troodos 1987": Nicosia, Cyprus, Ministry of Agriculture and Natural Resources, p. 99–111.
- Allerton, S., and Vine, F.J., 1991, Spreading evolution of the Troodos ophiolite, Cyprus: *Geology*, v. 19, p. 637–640, doi:10.1130/0091-7613(1991)019<0637:SEOTTO>2.3.CO;2.
- Allerton, S., and Vine, F.J., 1992, Deformation styles adjacent to transform faults: Evidence from the Troodos ophiolite, Cyprus, in Parson, L.M., Murton, B.J., and Browning, P., eds., *Ophiolites and their Modern Oceanic Analogues*: Geological Society of London Special Publication 60, p. 251–261.
- Anonymous, 1972, Penrose Field Conference on ophiolites: *Geotimes*, v. 17, p. 24–25.
- Bear, L.M., 1960, Geological Map of the Akaki-Lythronodnda Area: Nicosia, Cyprus Geological Survey, scale 1:31,680, 2 sheets.
- Bear, L.M., and Carr, J.M., 1960, Geological Map of the Peristerona-Lagoudera Area: Nicosia, Cyprus Geological Survey, scale 1:31,680, 2 sheets.
- Bear, L.M., and Morel, S.W., 1960, Geological Map of the Agros-Apsiou Area: Nicosia, Cyprus Geological Survey, scale 1:31,680, 2 sheets.
- Behn, M.D., Lin, J., and Zuber, M.T., 2002, Evidence for weak oceanic transform faults: *Geophysical Research Letters*, v. 29, doi:10.1029/2002GL015612.
- Behn, M.D., Boettcher, M.S., and Hirth, G., 2007, Thermal structure of oceanic transform faults: *Geology*, v. 35, p. 307–310, doi:10.1130/G23112A.1.
- Bishop, D.W., Wilson, R.A.M., Burdon, D.J., and Carr, J.M., 1959, Geological Map of the Xeros-Troodos Area: Nicosia, Cyprus Geological Survey, scale 1:31,680, 2 sheets.
- Blome, C.D., and Irwin, W.P., 1985, Equivalent radiolarian ages from ophiolitic terranes of Cyprus and Oman: *Geology*, v. 13, p. 401–404, doi:10.1130/0091-7613(1985)13<401:ERAFOT>2.0.CO;2.
- Bonhommet, N., Roperch, P., and Calza, F., 1988, Paleomagnetic arguments for block rotations along the Arakapas fault (Cyprus): *Geology*, v. 16, p. 422–425, doi:10.1130/0091-7613(1988)016<0422:PAFBRA>2.3.CO;2.
- Clube, T.M.M., and Robertson, A.H.F., 1986, The palaeorotation of the Troodos microplate, Cyprus, in the late Mesozoic-early Cenozoic plate tectonic framework of the eastern Mediterranean: *Surveys in Geophysics*, v. 8, p. 375–437, doi:10.1007/BF01903949.
- Clube, T.M.M., Creer, K.M., and Robertson, A.H.F., 1985, Palaeorotation of the Troodos microplate, Cyprus: *Nature*, v. 317, p. 522–525, doi:10.1038/317522a0.
- Crane, K., 1976, The intersection of the Siqueiros transform fault and the East Pacific Rise: *Marine Geology*, v. 21, p. 25–46, doi:10.1016/0025-3227(76)90102-X.
- Croon, M.B., Cande, S.C., and Stock, J.A., 2010, Abyssal hill deflections at Pacific-Antarctic ridge-transform intersections: *Geochemistry, Geophysics, Geosystems*, v. 11, Q11004, doi:10.1029/2010GC003236.
- Davis, J.R., and Titus, S.J., 2011, Review article: Computational techniques in homogeneous steady deformations: *Journal of Structural Geology*, v. 33, p. 1046–1062, doi:10.1016/j.jsg.2011.03.001.
- Dilek, Y., Thy, P., Moores, E.M., and Ramsden, T., 1990, Tectonic evolution of the Troodos ophiolite within the Tethyan framework: *Tectonics*, v. 9, p. 811–823, doi:10.1029/T009i004p00811.
- Fornari, D.J., Gallo, D.G., Edwards, M.H., Madsen, J.A., Perfit, M.R., and Shor, A.N., 1989, Structure and topography of the Siqueiros transform fault system; evidence for the development of intra-transform spreading centers: *Marine Geophysical Researches*, v. 11, p. 263–299.
- Fox, P.J., and Gallo, D.G., 1984, A tectonic model for ridge-transform-ridge plate boundaries: Implications for the structure of oceanic lithosphere: *Tectonophysics*, v. 104, p. 205–242, doi:10.1016/0040-1951(84)90124-0.
- Fujita, K., and Sleep, N.H., 1978, Membrane stresses near mid-ocean ridge-transform intersections: *Tectonophysics*, v. 50, p. 207–221, doi:10.1016/0040-1951(78)90136-1.
- Furlong, K.P., Sheaffer, S.D., and Malservigi, R., 2001, Thermal-rheological controls on deformation within oceanic transforms, in Holdsworth, R.E., Strachan, R.A., Magloughlin, J., and Knipe, R.J., eds., *The Nature and Tectonic Significance of Fault Zone Weakening*: Geological Society of London Special Publication 186, p. 65–84.
- Gass, I.G., 1968, Is the Troodos massif of Cyprus a fragment of Mesozoic ocean floor?: *Nature*, v. 220, p. 39–42, doi:10.1038/220039a0.
- Gass, I.G., 1990, Ophiolites and oceanic lithosphere, in Malpas, J., Moores, E.M., Panayiotou, A., and Xenophontos, C., eds., *Ophiolites, Oceanic Crustal Analogues: Proceedings of the Symposium "Troodos 87"*: Nicosia, Cyprus, Ministry of Agriculture and Natural Resources, p. 1–12.
- Gass, I.G., MacLeod, C.J., Murton, B.J., Panayiotou, A., Simonian, K.O., and Xenophontos, C., 1994, The Geology of the Southern Troodos Transform Fault Zone: Nicosia, Cyprus, Geological Survey Department, 218 p.
- Granot, R., Abelson, M., Ron, H., and Agnon, A., 2006, The oceanic crust in 3D: Paleomagnetic reconstruction in the Troodos ophiolite gabbro: *Earth and Planetary Science Letters*, v. 251, p. 280–292, doi:10.1016/j.epsl.2006.09.019.
- Grindlay, N.R., and Fox, P.J., 1993, Lithospheric stresses associated with nontransform offsets of the Mid-Atlantic Ridge: Implications from a finite element analysis: *Tectonics*, v. 12, p. 982–1003, doi:10.1029/93TC00364.
- Gudmundsson, A., 1995, Stress fields associated with oceanic transform faults: *Earth and Planetary Science Letters*, v. 136, p. 603–614, doi:10.1016/0012-821X(95)00164-8.
- Hall, L.S., Lamb, S.H., and Mac Niocaill, C., 2004, Cenozoic distributed rotation deformation, South Island, New Zealand: *Tectonics*, v. 23, TC2002, doi:10.1029/2002TC001421.
- Hurst, S.D., Verosub, K.L., and Moores, E.M., 1992, Paleomagnetic constraints on the formation of the Solea graben, Troodos ophiolite, Cyprus: *Tectonophysics*, v. 208, p. 431–445, doi:10.1016/0040-1951(92)90439-D.
- Hurst, S.D., Moores, E.M., and Varga, R.J., 1994, Structural and geophysical expression of the Solea graben, Troodos ophiolite, Cyprus: *Tectonics*, v. 13, p. 139–156, doi:10.1029/93TC02066.
- Jancin, M., Young, K.D., Voight, B., and Orkan, N.I., 1995, Dikes, minor faults and mineral veins associated with a transform fault in North Iceland: *Journal of Structural Geology*, v. 17, p. 1627–1631, doi:10.1016/0191-8141(95)00073-M.
- Jones, C.H., 2002, User-driven integrated software lives: "PaleoMag" paleomagnetism analysis on the Macintosh: *Computers & Geosciences*, v. 28, p. 1145–1151, doi:10.1016/S0098-3004(02)00032-8.
- Karson, J., 1999, Geological investigation of a lineated massif at the Kane transform fault: Implications for oceanic core complexes: *Philosophical Transactions of the Royal Society of London, ser. A, Mathematical and Physical Sciences*, v. 357, p. 317–340.
- Kidd, R.G.W., and Cann, J.R., 1974, Chilling statistics indicate an ocean-floor spreading origin for the Troodos complex, Cyprus: *Earth and Planetary Science Letters*, v. 24, p. 151–155, doi:10.1016/0012-821X(74)90020-X.
- Kirschvink, J.L., 1980, The least-squares line and plane and the analysis of palaeomagnetic data: *Geophysical Journal of the Royal Astronomical Society*, v. 62, p. 699–718, doi:10.1111/j.1365-246X.1980.tb02601.x.
- Lamb, S., 1987, A model for tectonic rotations about a vertical axis: *Earth and Planetary Science Letters*, v. 84, p. 75–86, doi:10.1016/0012-821X(87)90178-6.
- Långbacka, B.O., and Gudmundsson, A., 1995, Extensional tectonics in the vicinity of a transform fault in North Iceland: *Tectonics*, v. 14, p. 294–306, doi:10.1029/94TC02904.
- Ligi, M., Bonatti, E., Gasperini, L., and Poliakov, A.N.B., 2002, Oceanic broad multifault transform plate boundaries: *Geology*, v. 30, p. 11–14, doi:10.1130/0091-7613(2002)030<0011:OBMTTP>2.0.CO;2.
- Livermore, R.A., Tomlinson, J.S., and Woollett, R.W., 1991, Unusual sea-floor fabric near the Bullard fracture zone imaged by GLORIA sidescan sonar: *Nature*, v. 353, p. 158–161, doi:10.1038/353158a0.
- MacDonald, K.C., Castillo, D.A., Miller, S.P., Fox, P.J., Kastens, K.A., Bonatti, E., and Detrick, R.S., 1986, Deep-tow studies of the Vema fracture zone: 1. Tectonics of a major slow-slipping transform fault and its intersection with the Mid-Atlantic Ridge: *Journal of Geophysical Research*, v. 91, p. 3334–3354, doi:10.1029/JB091iB03p03334.
- MacLeod, C.J., 1990, Role of the Southern Troodos transform fault in the rotation of the Cyprus microplate: Evidence from the eastern Limassol Forest Complex, in Malpas, J., Moores, E.M., Panayiotou, A., and Xenophontos, C., eds., *Ophiolites, Oceanic Crustal Analogues: Proceedings of the Symposium "Troodos 87"*: Nicosia, Cyprus, Ministry of Agriculture and Natural Resources, p. 75–85.
- MacLeod, C.J., and Murton, B.J., 1993, Structure and tectonic evolution of the Southern Troodos transform fault zone, Cyprus, in Prichard, H.M., Alabaster, T., Harris, N.B.W., and Neary, C.R., eds., *Magmatic Processes and Plate Tectonics*: Geological Society of London Special Publication 76, p. 141–176.
- MacLeod, C.J., and Murton, B.J., 1995, On the sense of slip of the Southern Troodos transform fault zone, Cyprus: *Geology*, v. 23, p. 257–260, doi:10.1130/0091-7613(1995)023<0257:OTSOSO>2.3.CO;2.
- MacLeod, C.J., Allerton, S., Gass, I.G., and Xenophontos, C., 1990, Structure of a fossil ridge-transform intersection in the Troodos ophiolite: *Nature*, v. 348, p. 717–720, doi:10.1038/348717a0.
- MacLeod, C.J., Escartin, J., Banerji, D., Banks, G.J., Gleeson, M., Irving, D.H.B., Lilly, R.M., McCaig, A.M., Niu, Y., Allerton, S., and Smith, D.K., 2002, Direct geological evidence for oceanic detachment faulting: The Mid-Atlantic Ridge, 15°45'N: *Geology*, v. 30, p. 879–882, doi:10.1130/0091-7613(2002)030<0879:DGEFOD>2.0.CO;2.
- Malpas, J., Calon, T., and Squires, G., 1993, The development of a Late Cretaceous microplate suture zone in SW Cyprus, in Prichard, H.M., Alabaster, T., Harris, N.B.W., and Neary, C.R., eds., *Magmatic Processes and Plate Tectonics*: Geological Society of London Special Publication 76, p. 177–195, doi:10.1144/GSL.SP.1993.076.01.08.
- McKenzie, D., and Jackson, J., 1983, The relationship between strain rates, crustal thickening, palaeomagnetism, finite strain and fault movements within a deforming zone: *Earth and Planetary Science Letters*, v. 65, p. 182–202, doi:10.1016/0012-821X(83)90198-X.
- Miyashiro, A., 1973, The Troodos ophiolitic complex was probably formed in an island arc: *Earth and Planetary Science Letters*, v. 19, p. 218–224, doi:10.1016/0012-821X(73)90118-0.
- Moores, E.M., and Vine, F.J., 1971, The Troodos massif, Cyprus, and other ophiolites as oceanic crust; evaluation and implications: *Philosophical Transactions of the Royal Society of London*, v. 268, p. 443–466.
- Moores, E.M., Robinson, P.T., Malpas, J., and Xenophontos, C., 1984, Model for the origin of the Troodos Massif, Cyprus, and other Mideast ophiolites: *Geology*, v. 12, p. 500–503, doi:10.1130/0091-7613(1984)12<500:MFTOOT>2.0.CO;2.
- Morris, A., Creer, K.M., and Robertson, A.H.F., 1990, Palaeomagnetic evidence for clockwise rotations related to dextral shear along the Southern Troodos transform fault, Cyprus: *Earth and Planetary Science Letters*, v. 99, p. 250–262, doi:10.1016/0012-821X(90)90114-D.
- Mukasa, S.B., and Ludden, J.N., 1987, Uranium-lead isotopic ages of plagiogranites from the Troodos ophiolite, Cyprus, and their tectonic significance: *Geology*, v. 15, p. 825–828, doi:10.1130/0091-7613(1987)15<825:UUAOPF>2.0.CO;2.
- Murton, B.J., 1986, Anomalous oceanic lithosphere formed in a leaky transform fault: Evidence from the western Limassol Forest Complex, Cyprus: *Journal of the Geological Society of London*, v. 143, p. 845–854, doi:10.1144/gsjgs.143.5.0845.
- Murton, B.J., 1990, Was the Southern Troodos transform fault a victim of microplate rotation?, in Malpas, J., Moores, E.M., Panayiotou, A., and Xenophontos, C., eds., *Ophiolites, Oceanic Crustal Analogues: Proceedings of the Symposium "Troodos 87"*: Nicosia, Cyprus, Ministry of Agriculture and Natural Resources, p. 87–98.
- Murton, B.J., and Gass, I.G., 1986, Western Limassol Forest Complex, Cyprus: Part of an Upper Cretaceous leaky transform fault: *Geology*, v. 14, p. 255–258, doi:10.1130/0091-7613(1986)14<255:WLFFCP>2.0.CO;2.
- Neves, M.C., Bott, M.H.P., and Searle, R.C., 2004, Patterns of stress at mid-ocean ridges and their offsets due to sea floor subsidence: *Tectonophysics*, v. 386, p. 223–242, doi:10.1016/j.tecto.2004.06.010.
- Nuriel, P., Katzir, Y., Abelson, M., Valley, J.W., Matthews, A., Spicuzza, M.J., and Ayalon, A., 2009, Fault-related oceanic serpentinization in the Troodos ophiolite, Cyprus: Implications for a fossil oceanic core complex: *Earth and Planetary Science Letters*, v. 282, p. 34–46.
- Pantazis, T.M., 1967, Geological Map of the Pharmakas-Kalvasos Area: Nicosia, Cyprus Geological Survey, scale 1:31,680, 2 sheets.

- Pearce, J.A., Lippard, S.J., and Roberts, S., 1984, Characteristics and tectonic significance of supra-subduction zone ophiolites, in Kokelaar, B.P., and Howells, M.F., eds., *Marginal Basin Geology: Volcanic and Associated Sedimentary and Tectonic Processes in Modern and Ancient Marginal Basins*: Geological Society of London Special Publication 16, p. 77–94, doi:10.1144/GSL.SP.1984.016.01.06.
- Phipps Morgan, J., and Parmentier, E.M., 1984, Lithospheric stress near a ridge-transform intersection: *Geophysical Research Letters*, v. 11, p. 113–116, doi:10.1029/GL0111002p00113.
- Prinzhofer, A., and Nicolas, A., 1980, The Bogota Peninsula, New Caledonia: A possible oceanic transform fault: *The Journal of Geology*, v. 88, p. 387–398, doi:10.1086/628523.
- Rahl, J.M., Brandon, M.T., Deckert, H., Ring, U., and Mortimer, N., 2011, Tectonic significant of ductile deformation in low-grade sandstones in the Mesozoic Otago subduction wedge, New Zealand: *American Journal of Science*, v. 511, p. 26–62.
- Robertson, A.H.F., 2002, Overview of the genesis and emplacement of Mesozoic ophiolites in the Eastern Mediterranean Tethyan region: *Lithos*, v. 65, p. 1–67, doi:10.1016/S0024-4937(02)00160-3.
- Robertson, A., and Xenophontos, C., 1993, Development of concepts concerning the Troodos ophiolite and adjacent units in Cyprus, in Prichard, H.M., Alabaster, T., Harris, N.B.W., and Neary, C.R., eds., *Magmatic Processes and Plate Tectonics*: Geological Society of London Special Publication 76, p. 85–119, doi:10.1144/GSL.SP.1993.076.01.05.
- Robinson, P.T., and Malpas, J., 1990, The Troodos ophiolite of Cyprus: new perspectives on its origin and emplacement, in Malpas, J., Moores, E.M., Panayiotou, A., and Xenophontos, C., eds., *Ophiolites, Oceanic Crustal Analogues: Proceedings of the Symposium "Troodos 87"*: Nicosia, Cyprus, Ministry of Agriculture and Natural Resources, p. 13–26.
- Robinson, P.T., Malpas, J., Dilek, Y., and Zhou, M.F., 2008, The significance of sheeted dike complexes in ophiolites: *GSA Today*, v. 18, no. 11, doi:10.1130/GSATG22A.1.
- Ron, H., Freund, R., Garfunkel, Z., and Nur, A., 1984, Block rotation by strike-slip fault: Structural and paleomagnetic evidence: *Journal of Geophysical Research*, v. 89, p. 6256–6270, doi:10.1029/JB089iB07p06256.
- Schouten, H., Karson, J., and Dick, H., 1980, Geometry of transform zones: *Nature*, v. 288, p. 470–473, doi:10.1038/288470a0.
- Searle, R.C., 1983, Multiple, closely spaced transform faults in fast-slipping fracture zones: *Geology*, v. 11, p. 607–610, doi:10.1130/0091-7613(1983)11<607:MCSTF>2.0.CO;2.
- Simonian, K.O., and Gass, I.G., 1978, Arakapas fault belt, Cyprus: A fossil transform fault: *Geological Society of America Bulletin*, v. 89, p. 1220–1230, doi:10.1130/0016-7606(1978)89<1220:AFBCAF>2.0.CO;2.
- Smewing, J.D., 1980, An Upper Cretaceous ridge-transform in the Oman ophiolite, in Panayiotou, A., ed., *Ophiolites: Proceedings, International Ophiolite Symposium, Cyprus 1979*: Nicosia, Cyprus, Cyprus Geological Survey Department, p. 407–413.
- Smith, D.K., Escartín, J., Schouten, H., and Cann, J.R., 2008, Fault rotation and core complex formation: Significant processes in seafloor formation at slow-spreading mid-ocean ridges (Mid-Atlantic Ridge, 13°–15°N): *Geochemistry, Geophysics, Geosystems*, v. 9, Q03003, doi:10.1029/2007GC001699.
- Sonder, L.J., and Pockalny, R.A., 1999, Anomalous rotated abyssal hills along active transforms: Distributed deformation of oceanic lithosphere: *Geology*, v. 27, p. 1003–1006, doi:10.1130/0091-7613(1999)027<1003:ARAHAA>2.3.CO;2.
- Sonder, L.J., England, P.C., and Houseman, G.A., 1986, Continuum calculations of continental deformation in transient environments: *Journal of Geophysical Research*, v. 91, p. 4797–4810, doi:10.1029/JB091iB05p04797.
- Sonder, L.J., Jones, C.H., Salyards, S.L., and Murphy, K.M., 1994, Vertical axis rotations in the Las Vegas Valley shear zone, southern Nevada: Paleomagnetic constraints on kinematics and dynamics of block rotation: *Tectonics*, v. 13, p. 769–788, doi:10.1029/94TC00352.
- Suhr, G., and Cawood, P.A., 2001, Southeastern Lewis Hills (Bay of Islands ophiolite): Geology of a deeply eroded, inside-corner, ridge-transform intersection: *Geological Society of America Bulletin*, v. 113, p. 1025–1038, doi:10.1130/0016-7606(2001)113<1025:SLHBOI>2.0.CO;2.
- Titus, S.J., Maes, S.M., Benford, B., Ferré, E.C., and Tikoff, B., 2011, Fabric development in the mantle section of a paleotransform fault and its effect on ophiolite obduction, New Caledonia: *Lithosphere*, v. 3, p. 221–244, doi:10.1130/L122.1.
- van Everdingen, D.A., and Cawood, P.A., 1995, Dyke domains in the Mitsero graben, Troodos ophiolite, Cyprus: An off-axis model for graben formation at a spreading centre: *Journal of the Geological Society of London*, v. 152, p. 923–932, doi:10.1144/GSL.JGS.1995.152.01.07.
- van Wijk, J.W., and Blackman, D.K., 2005, Deformation of oceanic lithosphere near slow-spreading ridge discontinuities: *Tectonophysics*, v. 407, p. 211–225, doi:10.1016/j.tecto.2005.08.009.
- Varga, R.J., 1991, Models of extension at oceanic spreading centers: Evidence from the Solea graben, Troodos ophiolite, Cyprus: *Journal of Structural Geology*, v. 13, p. 517–537, doi:10.1016/0191-8141(91)90041-G.
- Varga, R.J., and Moores, E.M., 1985, Spreading structure of the Troodos ophiolite, Cyprus: *Geology*, v. 13, p. 846–850, doi:10.1130/0091-7613(1985)13<846:SSOTTO>2.0.CO;2.
- Young, K.D., Jancin, M., Voight, B., and Orkan, N.I., 1985, Transform deformation of Tertiary rocks along the Tjörnes fracture zone, north central Iceland: *Journal of Geophysical Research*, v. 90, p. 9986–10,010.

MANUSCRIPT RECEIVED 27 JUNE 2012
 REVISED MANUSCRIPT RECEIVED 20 SEPTEMBER 2012
 MANUSCRIPT ACCEPTED 24 SEPTEMBER 2012

Printed in the USA